İZMİR KÂTİP ÇELEBİ ÜNİVERSİTESİ
2010
GRADUATE SCHOOL OF NATURAL AND APPLIED SCIENCES

# Recycling of Ti-6Al-4V Alloy Chip and Its Potential Uses in Polymer Composites

Doctor of Philosophy

in Materials Science and Engineering

by

Erdoğan Teke

ORCID 0000-0001-9840-8060

December, 2022

This is to certify that we have read the thesis **Recycling of Ti-6Al-4V Alloy Chip and Its Potential Uses in Polymer Composites** submitted by **Erdoğan Teke**, and it has been judged to be successful, in scope and in quality, at the defense exam and accepted by our jury as a DOCTORAL THESIS.

**APPROVED BY:**

**Advisor:** **Prof. Dr. Mehmet Özgür Seydibeyoğlu**
İzmir Kâtip Çelebi University

**Committee Members:**

**Prof. Dr. İbrahim Etem Saklakoğlu**
Ege University

**Assoc. Prof. Dr. Onur Ertuğrul**
İzmir Kâtip Çelebi University

**Assoc. Prof. Dr. Mehmet Sarıkanat**
Ege University

**Assist. Prof. Dr. Aydın Ülker**
İzmir Kâtip Çelebi University

**Date of Defense: December 29, 2022**

# Declaration of Authorship

I, **Erdoğan Teke**, declare that this thesis titled **Recycling of Ti-6Al-4V Alloy Chip and Its Potential Uses in Polymer Composites** and the work presented in it are my own. I confirm that:

- This work was done wholly or mainly while in candidature for the Doctoral degree at this university.
- Where any part of this thesis has previously been submitted for a degree or any other qualification at this university or any other institution, this has been clearly stated.
- Where I have consulted the published work of others, this is always clearly attributed.
- Where I have quoted from the work of others, the source is always given. This thesis is entirely my own work, with the exception of such quotations.
- I have acknowledged all major sources of assistance.
- Where the thesis is based on work done by myself jointly with others, I have made clear exactly what was done by others and what I have contributed myself.

Date: 29.12.2022

Recycling of Ti-6Al-4V Alloy Chip and Its Potential Uses in Polymer Composites

# Abstract

The increasing world population leads to an increase in the need for raw materials. Therefore, the transition from a linear economy with a disposable culture to a circular economy where waste plastics are efficiently reused is imperative. Circular economy, which is an economic and industrial system, aims to eliminate waste through restorative use of resources.

The aim of this thesis is based on the mechanical pulverization of Ti-6Al-4V chip, the investigation of recycled Ti-6Al-4V powders as reinforcement materials, and the development of mechanical properties of epoxy and polyester composite.

This thesis focuses on the recovery of Ti-6Al-4V chip collected from the medical implant industry into micronized powder using the milling process. The effect of milling parameters on the particle size and morphology of Ti-6Al-4V powder produced using vibratory disc milling was investigated. To accomplish this, Ti6Al4V chip were milled at various milling duration, milling speed and atmosphere in a vibratory disc mill. The effects of two different milling atmospheres, argon and air, were investigated. The particle filled polymer composites are developed using recycled Ti6Al4V powder. Mechanical properties, thermal properties, and microstructure of the polymer composites were investigated.

**Keywords:** Titanium chip, recycling, metal powder, epoxy, polyester

# Ti-6Al-4V Talaşların Geri Dönüşümü ve Polimer Kompozitlerde Potansiyel Kullanımı

# Öz

Artan dünya nüfusu beraberinde hammadde ihtiyacının artmasına sebep olmaktadır. Bu nedenle, kullan-at kültürüne sahip doğrusal bir ekonomiden, atık plastiklerin verimli bir şekilde yeniden kullanıldığı döngüsel bir ekonomiye geçiş zorunludur. Döngüsel ekonomi kaynakların onarıcı kullanımı yoluyla israfı ortadan kaldırmayı amaçlamaktadır.

Bu tezin amacı, Ti-6Al-4V atıklarının mekanik öğütme yöntemiyle toz haline dönüştürülmesi, geri dönüştürülmüş Ti-6Al-4V tozlarının takviye malzemesi olarak araştırılması, epoksi ve polyester kompozit özelliklerinin geliştirilmesine dayanmaktadır. Bu tez, tıbbi implant endüstrisinden toplanan titanyum atık talaşların mekanik öğütme yöntemi kullanılarak micron boyutlarında toz haline getirilmesine odaklanmaktadır. Öğütme parametrelerinin, titreşimli diskli öğütme kullanılarak üretilen Ti6Al4V tozunun parçacık boyutu ve morfolojisi üzerindeki etkisi araştırıldı. Ti6Al4V talaşları, titreşimli bir diskli öğütme sisteminde çeşitli öğütme sürelerinde, hızlarında ve atmosferlerinde öğütüldü. Argon ve hava olmak üzere iki farklı öğütme atmosferinin etkisi incelenmiştir. Partikül dolgulu polimer kompozitler, geri dönüştürülmüş Ti6Al4V tozu kullanılarak geliştirilmiştir. Polimer kompozitlerin çekme dayanımı, eğilme dayanımı ve mikroyapısı gibi mekanik özellikleri incelenmiştir.

**Anahtar Kelimeler:** Titanyum talaş, geri dönüşüm, metal tozu, epoksi, polyester

# Acknowledgment

First and foremost, I would like to grant special appreciation to my supervisor Prof. Dr. M. Özgür Seydibeyoğlu for his tremendous support with sharing his knowledge and experience. I learned a lot from him both from humanity and on the scientific point of view.

I also would like to express my gratitude to Assist. Prof. Dr. Aydın Ülker and Assoc. Prof. Dr. Onur Ertuğrul. They were available all the time for discussion and my questions. Our discussions were beneficial for the progress and improvement of the thesis work.

I am also grateful to my family for their supports. They have always been with me all my life and I became who I am today.

To all of you, Thank you.

# Table of Contents

# List of Figures

# List of Tables

# List of Abbreviations

| | |
|---|---|
| Al | Aluminum |
| $Al_2O_3$ | Aluminum Oxide or Alumina |
| AlN | Aluminum Nitride |
| ASTM | American Society for Testing and Materials |
| BCC | Body-Centered Cubic |
| BN | Boron Nitride |
| CNC | Computer Numerical Control |
| Cu | Copper |
| DIN | Deutsches Institut für Normung |
| EDX | Energy Dispersive X-ray Spectroscopy |
| g | Gram |
| HCP | Hexagonal Close-Packed |
| HDPE | High Density Polyethylene |
| kg | Kilogram |
| m | Meter |
| mg | Miligram |
| Min | Minute |
| mm | Milimeter |
| N | Nitrogen |
| O | Oxygen |
| PLA | Polylactic Acid |
| PM | Powder Metallurgy |
| PP | Polypropylene |
| PS | polystyrene |
| PVC | polyvinyl chloride |

| | |
|---|---|
| Rpm | Revolutions per Minute |
| S | Second |
| SEM | Scanning Electron Microscopy |
| SiC | Silicon Carbide |
| $SiO_2$ | Silicon Dioxide or Silica |
| TGA | Thermogravimetric Analysis |
| Ti | Titanium |
| Ti64 | Ti6Al4V |
| $TiO_2$ | Titanium Oxide or Titania |
| wt | Weight |
| XPS | X-ray Photoelectron Spectroscopy |
| XRD | X-Ray Diffraction |
| ZnO | Zinc Oxide |
| μm | Micronmeter |

# List of Symbols

| | |
|---|---|
| N | Newton |
| Å | Angstrom |
| α | Alpha Phase |
| β | Beta Phase |
| D | Mean Size of Crystallite Size |
| K | Crystallite-Shape Factor |
| λ | X-Rays Wavelength |
| Θ | Diffraction Angle in Radians |
| β | Full Width at Half Maximum Intensity |
| W/mK | Watts per Meter Kelvin |
| σ | Standard Deviation |

# Chapter 1

# Introduction

The need for composite materials is growing and new materials for the composite world are needed. The use of light-weight materials is one of the top priority topics in many applications and the class of composites is a good solution to this issue. In this chapter, a brief introduction to composite materials is presented. Detailed investigations of different class of composites are explained in detail.

## 1.1 Polymer Composite Materials

Composite materials having two components as reinforcement and matrix phase are defined as a combination of at least two different materials. The most important advantages of composite materials are their mechanical properties such as their high strength and stiffness, low density and providing for a weight reduction in the finished part, when compared with bulk materials [1]. The matrix phase may be metal, ceramic or polymer material. Polymer matrix composite (PMC) is the material containing a resin matrix combined with a reinforcing dispersed phase [2]. Thermosets and thermoplastics are two main kinds of polymers. Thermoplastic polymers that can be used more than once are melt easily and often solvent soluble. Thermoset polymers that cannot be used more than once are heavily cross linked, infusible and also insoluble in solvents [3].

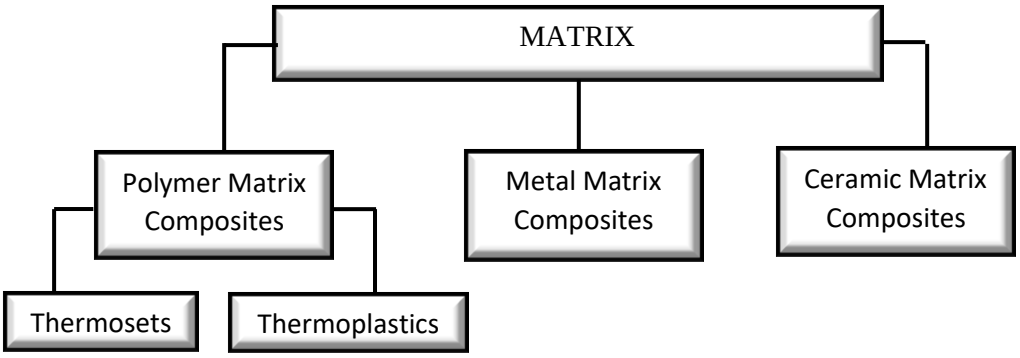


Figure 1.1: Classification of composites based on matrix type

A fiber or a particulate is usually used the reinforcement. Fibers or particles reinforced in the matrix of another material would be the best example of modern day composite materials. Large-particle and dispersion-strengthened composites are the two sub-classifications of particle reinforced composites. The distinction between these is based on the reinforcement or strengthening mechanism. For most of these composites, the particulate phase is harder and stiffer than the matrix. For dispersion-strengthened composites, particles are much smaller (10 to 100 nm) whereas for large-particle reinforced composites the particles are micro-sized [4].

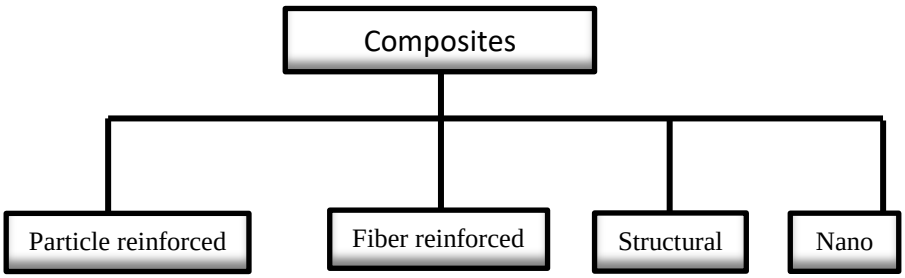


Figure 1.2: Classification of composites based on reinforced type

### 1.1.1 Particle Reinforced Polymer Composites

As a result of modern technology, there are need new materials that have a lightweight, high modulus, toughness and stable against the environment in instead of using metals and alloys in different industries in the world. With the advent of new technologies, there is a great need for materials with advanced properties [5].

Nowadays, due to the increasing interest in lightweight and high performance materials, important researches are being made in the area of composite materials. A new focus area is both to achieve low density and to develop multifunctional composites that have more than one property tailored as per the design requirements. Automotive, aerospace and wind energy sectors are considered as the main users of composite materials [6]. Various polymer matrix composites are reinforced with metal particles. Particulate fillers are preferred to change the physical and mechanical properties of polymers in many ways [7].

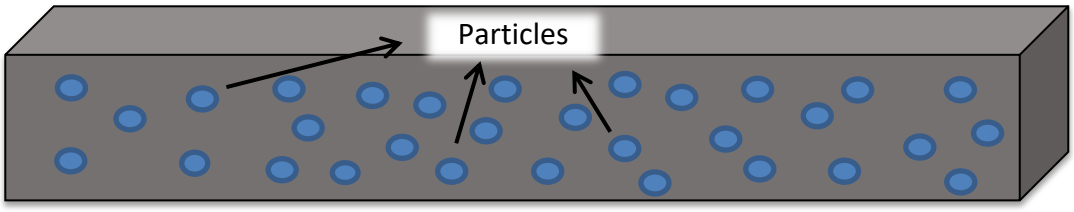


Figure 1.3: Particle reinforced composite

Reinforced materials like talc, mica, wood dust, sand, silica, alumina, metal flakes, and metal powder are normally used to modify the creep, impact, thermal, electrical and magnetic properties in polymer composites [8]. The particle shape, size and surface area of such added particles affect mechanical properties of the composites [7]. The reinforcements are typically hard, stiff materials usually of glass, ceramics or metals whereas the matrix materials are generally ductile and tough like polymers but brittle matrices are also used [5].

### 1.1.2 The Characteristics of Particles

Particulates of various shapes and sizes are used as reinforcing particles. Various physical parameters such as particle size, shape and chemical composition are used to characterize powder however these parameters also affect its flowability. Mechanical properties of the materials are affected by not only chemical composition but also the particle shape, size and surface area of such added particles [9]. Particle size distribution of powders plays a significant role in determining the critical chemical and physical properties of the particulate systems [10]. When the particle size decreases, the surface area increases and the reaction time is shortened. The surface area is increased as the particle size becomes small and also increased if the particle has pores [11]. Particles have complex geometric features such as dendritic,

rounded, spherical, angular, platy, acicular, cylindrical, cubic [12]. The relations between measured sizes and particle volume or surface area are called shape coefficients [13].

In Fig. 1.4, lists properties that can be used to create various functionalities in the PMC. The improving of lightweight polymer composites with functional properties and high performance is not so easy and studies are continuing in this area. The improving of functioning capabilities in the base material can reduce the requirements for additional systems on the application platform and can help in reducing the weight. As an example, an engine block is required to have high dimensional stability at high-low temperatures, fatigue life, wear resistance and also low weight. Such complex requirements reveal the development of multifunctional materials, which is a significant focus area of research [6].

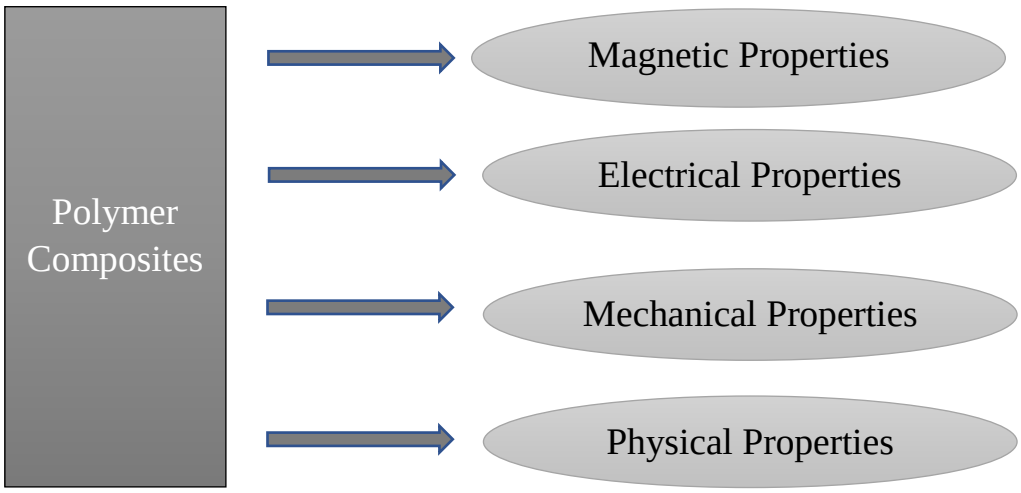


Figure 1.4: Various functionalities in polymer matrix composite

Some metals have special properties such as electrical, thermal and magnetic properties. Metal particles have a significant effect on improving the electrical, mechanical, magnetic and thermal properties of composites [14, 15]. Copper particles, brass particles, steel particles, zinc particles, aluminum particles, bronze particles are the most commonly used materials as fillers. The reinforcing of a polymer with metallic particles results in an increase in both electrical and thermal conductivity of the composites. As an example, due to aluminum has high electrical and thermal conductivity it can be used to impart electrical conductivity to the polymer composite and to improve thermal conductivity of the composite.

Polymer composites are playing a growing role as a wide range of applications including construction materials. In addition, they are becoming an important alternative for metals in applications related to the aerospace, automotive, marine, sporting goods and electronics industries. Their light weight and superior mechanical and electrical are particularly suitable for some of these applications [16].

### 1.1.3 Metal Reinforcements in Polymer Composites

Metal reinforcements are used to improve the mechanical, electrical, magnetic, physical and several other properties of both thermoset (epoxy, phenolic, polyester, silicone, bismaleimide, polyimide, polybenzimidazole, etc.) and thermoplastic (polyethelene, polystyrene, polyamides, nylon, polycarbonates, polysulfaones, etc.) materials.

Tekçe et al. [17] investigated thermal properties of copper-reinforced polyamide composites in the range of filler content 0–30% by volume for particle shape of short fibers and 0–60% by volume for particle shapes of plates and spheres. Different particle shapes (plates, fibers, spherical) of copper powders were used as conductive fillers. According to this, the composite's thermal conductivity is increased by the addition of copper fillers. According to study of Tekçe, copper fiber is the most effective agent on the thermal conductivity of the composite.

The electrical conductivity of plastics can be improved by metal filler particles. Two methods are available for provide electrical conductivity to plastics: (i) metal coating of the surface, (ii) adding conductive fillers into the polymer matrix. Amoabeng and Velankar [18] studied the electrical conductivity of polystyrene by simultaneously adding copper particles (30-80 micron), and a lead/tin solder alloy (15-25 micron). In Bigg's study [19], the electrical resistivity, thermal conductivity, and tensile strength of aluminum fiber filled polypropylene were investigated. Electrical and thermal conductivity increased while tensile strength decreased. Mohammed [5] studied mechanical behavior of copper powder reinforced epoxy. Found that increasing the weight ratio of copper powder to epoxy for different particle sizes achieves to an increase in elasticity, rigidity, tensile yield stress and ultimate tensile strength. In addition, the compression yield stress, fracture energy, and the impact strength

decreased due to increasing weight ratio of copper powder to epoxy with different particle size.

## 1.2 Ti6Al4V Alloy

The allotropic transformation of titanium from HCP α-Ti phase to BCC β-Ti phase at temperatures of 882 ± 2 ºC and above provides an opportunity for the formation of α, β or α+β microstructures in addition to the formation of compounds with some alloying. The realization of this crystallographic diversity with the addition of alloying elements and subjecting them to thermomechanical processes are effective in the development of a wide variety of alloys and properties. Titanium alloys, which are especially preferred in aerospace applications, have tensile strength; creep and fatigue strength; fracture toughness; It contains α and β stabilizing elements to obtain the necessary mechanical properties such as fatigue cracking, stress-abrasion cracking and resistance to oxidation [20-22]. Titanium, which is one of the transition metals due to its electronic structure, provides an opportunity for many alloying possibilities by forming solid solutions with its elements due to its atomic size factor. In addition, Ti reacts strongly with interstitial elements such as nitrogen, oxygen and hydrogen at temperatures below its melting point. Titanium can form metallic, covalent or ionic bonded compounds or solid solutions with other elements [23, 24].

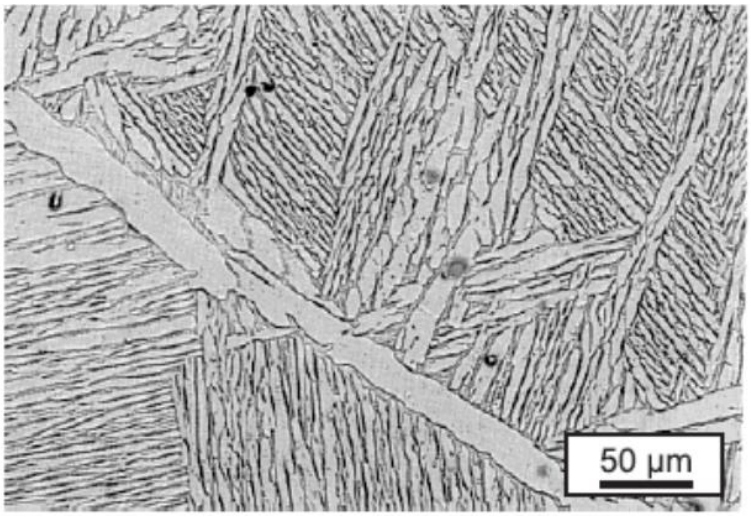


Figure 1.5: α+β lamellar microstructure of Ti64 alloy [24]

The choice of alloying elements is determined by the element's ability to stabilize the α or β phases. Accordingly, alloying elements are divided into 3 classes: α-

stabilizers, β-stabilizers and neutral alloying elements. Elements classified as α-stabilizers pull the transformation temperature to higher temperatures and stabilize the α-phase over a wider range, while β-stabilizer elements lower the transformation temperature. When eutectoid transformation occurs, these stabilizers are added to the β-eutectoid stabilizer; otherwise it is called a β-isomorph stabilizer. Neutral alloying elements, on the other hand, have a negligible low effect on the β transformation temperature [23-25].

# Chapter 2

# Effect of Milling Parameters on Recycled Ti6Al4V Powder Properties from Machining Chip Using Vibratory Disc Milling

## 2.1 Introduction

The recent increases in the consumption of natural raw material resources as a result of overproduction and the emergence of environmental problems due to industrial wastes generated during production processes have increased the importance of metal waste recovery. Metallic titanium production is limited in volume due to the high production cost of the current Ti-metal melting process. Also, titanium is known as a rare metal. The production volume of Titanium (global industry in 2015 roughly 0.18 Mt) is considerably lower than aluminum, iron, and copper. The Kroll process, the first large-scale industrial titanium production method, was developed in the 1940s; however, the manufacturing technology is still in the early stages of development. Therefore, the search for technological innovation continues to increase the production volume of titanium. In addition, titanium can partly replace stainless steel with the cost of production drops, causing a significant increase in its demand. For this reason, if the amount of production can be increased by technical innovations and recycling, titanium is considered a material of the future, making it a widespread metal [22, 26, 27].

It is critical from both an economic and environmental standpoint that the waste chip generated during the machining of titanium alloys, which are widely utilized in aviation and biomedical applications, can be recovered in powder form without melting by the grinding method. Recycling Ti-alloy scraps or chip into metallic powder benefits the environment by reducing energy use, waste volume, and emissions. Powder metallurgy (PM) is a conventional manufacturing method whose technology utilizes metal powders. The majority of metal particles used in PM have a diameter of between 5 and 200 μm. The powder characteristics are determined by the method by which it is manufactured. The flowability, surface area, particle shape, and size distribution of the powder are all dependent on their production method. There are three main methods of powder production: Mechanical, chemical, and atomization [28-31]. These methods comprise grinding (for brittle material), machining, atomization of liquid metal using water, gas (nitrogen, argon, or a mixture of these), and reduction of metal oxides using carbon or hydrogen. Each of these methods provides different particle morphology and characteristics. To ensure repeatable production of metal parts, metal powders must exhibit compatible powder properties. The main characteristics of powders used in additive manufacturing are the size (granulometry) and shape (morphology) of the particle. In addition, other characteristics contain density, elemental composition, flowability, surface area, and compressibility [32-34]. The mechanical method is the least expensive of the powder production methods. The milling method, which is a type of mechanical method and is very efficient for reducing the particle size of materials in the form of chip, involves the use of mechanical forces like compression force, shear or impact. During grinding, impact, abrasion, shear, and compression forces act on the particles. The particles are divided into fine particles by the pressing effect of the compression force type [29, 30]. Titanium and titanium alloys are extensively employed in a diversity of industries, containing marine, aerospace, medical, military and automotive, due to their good mechanical, physical, and chemical qualities [35-37]. The primary advantages of utilizing titanium and its alloys are their high strength-to-weight ratio, lightweight, and oxidation resistance. The tensile and flexural strengths of titanium are comparable to steel, although its density is only about 60% of that of steel [37, 38]. The most commonly used titanium alloy is Ti6Al4V (commonly used as Ti64), an α+β alloy with high toughness and operating temperature, low density, excellent corrosion resistance, and biocompatibility [39, 40]. Titanium-based

products are commonly subjected to CNC machining because they mostly require a smooth surface finish. During the machining of bar-type titanium raw materials, titanium scrap is generated in the form of solid pieces or chip. These waste chip typically contain a combination of cutting lubricants and oil or grease generated during the machining process [41]. In the milling processes, the removal of lubricant impurities from these metal scraps is an important stage in the surface cleaning process. These pretreatments directly affect the characteristics of the materials to be produced during the recycling process. Therefore, scrap surface cleaning operations, which can be costly and difficult, are important. Some researchers have successfully implemented mechanical milling to produce Ti-based powders. This method consists of several stages including high-energy milling, cold welding, deformation hardening, and fracturing. Controlling the powder size is one of the most significant advantages of this method [42]. Wang et al. [43] examined the use of high-energy ball milling for milling pure Ti powder. The particle size of Ti64 powder decreases as the milling duration increases due to the mechanical forces generated during ball milling. Dikici and Sütçü [44] studied mechanical disc milling for the production of Ti64 powder from a machining chip and concluded that the milling duration and speed had a remarkable impact on the particle size and morphology of Ti64 powders. Soufiani et al. [45] fabricated Ti64 powder from machining scraps by ball milling. In their study, mechanical milling was stated to be an efficient and economically viable method of recycling Ti64 scrap. They reported that with increasing milling duration, the particles turn into spherical shape as a result of repetitive cold welding, fracture, and plastic deformation. Titanium metal, on the other hand, is highly explosive in fine powder form. Therefore, it is critical to avoid milling with the jar cover open. As a result, it is necessary to form an inert atmosphere to prevent the accumulation of sparks. Argon gas is consumed to prevent the reaction of titanium with oxygen [46]. In this study, Ti64 powder was produced from chip through vibratory disc milling. The effects of milling speed, duration, and atmosphere (argon or air) on powder properties were investigated. This study also aids in predicting the potential usage of these powders in powder metallurgy, coatings, and additive manufacturing by characterizing the properties of recycled Ti64 powder.

## 2.2 Materials and Method

In this study, Ti64 alloy scraps were utilized as the basic materials, which were obtained in the chip form following CNC machining. The machining chip were supplied by Metrosan Company in Manisa, Turkey. In this study, mechanical milling was used to ground the chip to powder. The disc milling process operates on the idea of impact and friction induced by centrifugal force. Particle size is reduced as a result of the impact and friction forces occurring on the sample. To remove coolant oil from the titanium chip prior to disc milling operations, they were cleaned with detergent, hot water, and ethyl alcohol (96% purity). The Ti64 alloy chip given in Fig. 2.1(a) were pre-milled to a micron-scale size using a vibratory disc mill at 1000 rpm for 1 min to ensure that each parameter had the same size. It is seen in Fig. 2.1(b) that the chip exhibited a leafy form. Afterward, pre-milled chip were cleaned in an ultrasonic bath with ethyl alcohol for 1 hour at room temperature. Following this cleaning process, the chip were dried in a vacuum furnace at 140 ℃ for 2 hours.


Figure 2.1: Type of machining Ti64 scrap generated (a) as-received chip, (b) pre-milled chip

The experimental method for milling the Ti64 chip was performed the usage of Retsch RS200 vibratory disc mill. The diameter of the grinding jar was 125 mm, the outer diameter of the middle ring was 105 mm, and the innermost grinding disc's diameter was 55 mm, as seen in Fig. 2.2.

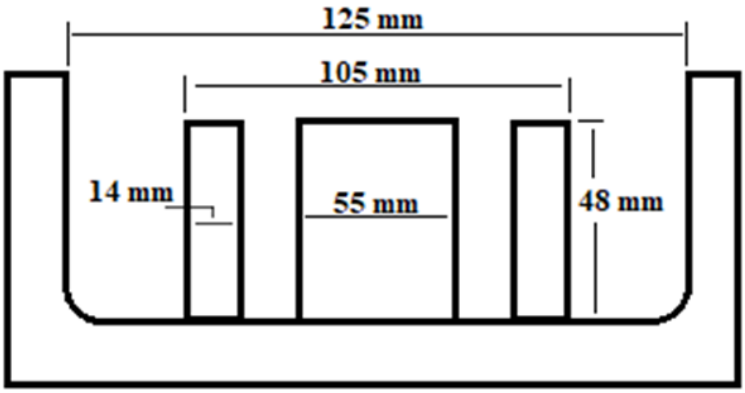


Figure 2.2: Schematic illustration of the grinding jar for vibratory disc milling

A grinding jar set made of DIN 2080 tool steel was used. 100 g of Ti64 chip were milled for each tested parameter. The quantity of powder was selected to complete half of the volume of the milling jar. The experimental conditions selected for the milling procedure were as follows; the milling speed - duration, and the atmosphere in which milling was performed. The effects of two different milling atmospheres, argon, and air, were investigated. The grinding jar was adapted to accommodate the inert gas supply. The gas inlet and outlet were connected to the grinding jar as given in Fig. 2.3. It was detected that the temperature of the grinding jar increased during the continuous milling process. When the temperature of the grinding jar increased, the powders began to cold weld. Therefore, the grinding jar was operated for 3 minutes and then allowed to cool.

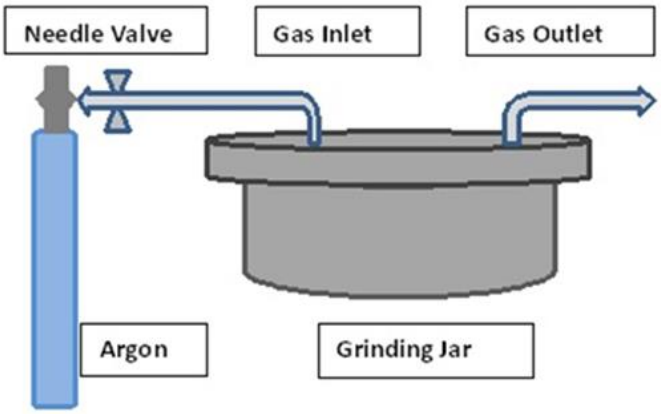


Figure 2.3: Schematic view of the grinding jar with argon gas: the gas inlet-outlet was placed top of the grinding jar connected to a needle valve

Prior to the beginning the milling process, the grinding jar was purged with argon gas for 2 minutes to eliminate any impurities. The needle valve ensured that the amount

of argon gas supplied in each parameter remained constant. It was observed during the milling process that as the amount of argon increased, the particle agglomeration increased. Consequently, a flow rate of 100 cc/min of argon gas was chosen for the grinding jar. In both atmospheres, milling durations of 30, 45, and 60 mins were selected and milling speeds of 1300 and 1500 rpm were used. The parameters for milling the chip are summarized in Table 2.1.

Table 2.1: Summary of disc milling parameters

| Sample code | Atmosphere | Duration (min.) | Rotation speed (rpm) |
|---|---|---|---|
| DAT1330 | Air | 30 | 1300 |
| DAR1330 | Argon | | |
| DAT1345 | Air | 45 | 1300 |
| DAR1345 | Argon | | |
| DAT1360 | Air | 60 | 1300 |
| DAR1360 | Argon | | |
| DAT1530 | Air | 30 | 1500 |
| DAR1530 | Argon | | |
| DAT1545 | Air | 45 | 1500 |
| DAR1545 | Argon | | |
| DAT1560 | Air | 60 | 1500 |
| DAR1560 | Argon | | |

## 2.3 Characterization Techniques

### 2.3.1 Particle Size Analysis

Particle size analysis of the milled powders that spread in a range of dry units were measured using Malvern Mastersizer 3000 instrument.

### 2.3.2 X-Ray Diffraction Analysis

The crystal structure of both chip and powders was performed with the use of Bruker D2 Phaser equipped with a CuKα radiation Nickel filter (λ: 1.5404). 30 kV and 10 mA X-ray diffraction were applied to obtain the required patterns. In addition to that,

the crystallite size of milled powders was determined from the x-ray diffraction using the Debye-Scherrer equation:

$$D=K\lambda/\beta\cos\Theta \quad (1)$$

where K (0,9) is the numerical factor frequently called the crystallite-shape factor, D is the mean size of crystallite size, λ is X-rays wavelength, β is full width at half maximum intensity (FWHM) of the peak in radians, and Θ is the diffraction angle in radians.

### 2.3.3 Scanning Electron Microscopy Analysis

Morphological and elemental investigations of the powders and chip were carried out using a Carl Zeiss 300VP scanning electron microscope (SEM).

### 2.3.4 Powder Flow Rate and Bulk Density Analysis

The Hall test was used to measure the flow rate of the metal powders. In the Hall method, time is measured using a stopwatch as 50 g of metal-powder flows through the funnel. Prior to the flow rate analysis, the powders were dehumidified in a vacuum oven at 80°C for 1 hour. Three separate batches of 50 g samples are poured into the funnel to provide an average total time that is necessary to calculate a valid flow rate. If the powder fails to flow through the funnel orifice, no time is recorded, implying that the powder is defective or non-flowing. In addition, the bulk density of the powders was measured by using a glass density bottle pycnometer.

### 2.3.5 X-ray photoelectron spectroscopy (XPS) Analysis

The XPS surface characterization of Ti64 chip was determined using a Thermo Scientific Kα spectrometer and a monochromatic aluminium X-ray source (1486.68 eV) with a 300 μm X-ray spot size.

## 2.4 Results and Discussion

### 2.4.1 The XPS Analysis of Ti64 Chip

The X-ray photoelectron spectroscopy was used to determine chemical composition of the titanium chip. The images of the X-ray spot sizes on the chip surface are given in figure 2.4. The XPS measurement was performed on both surfaces of the Ti64 chip. High resolution survey spectrums of the chip were acquired at a pass energy of 50 eV.

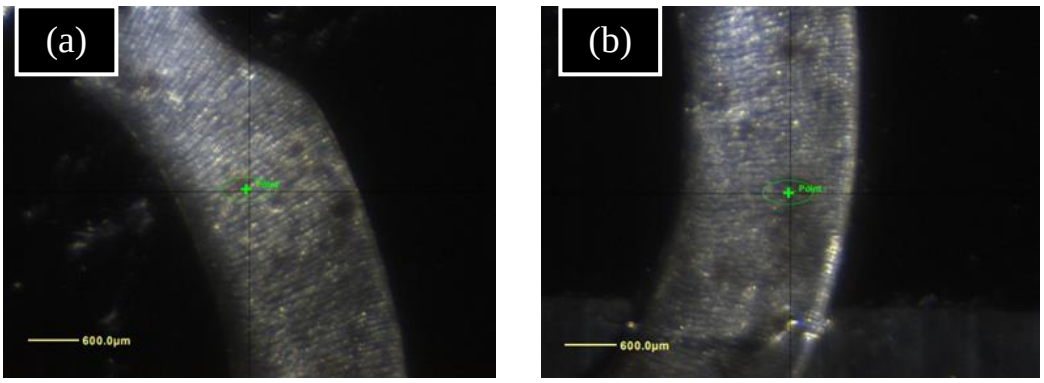


Figure 2.4: The X-ray spots of Ti64 chip: upper surface (a), bottom surface (b)

Figure 2.5 show the high resolution surface spectrum of Ti2p, C1s and O1s. The peaks observed in the Ti2p core level spectra shows two components $Ti2p_{1/2}$ and $Ti2p_{1/2}$ which shows binding energy at 458.4 eV and 464.4 eV, respectively (Fig. 2.5a). These peaks of Ti2p are corresponding to valance state of $Ti^{4+}$ cation [47-49]. The $Ti2p_{3/2}$ and $Ti2p_{1/2}$ peaks shows the 6 eV energy separations, confirmed the strong bonding between Ti and O atoms [50]. The peaks of C1s (Fig. 2.5b) at 284.8, 286.6 and 288.4 eV are attributed to C – C, C – O and O = C – O, respectively. The O1s peak can be separated into two peaks (Fig. 2.5c). the peaks at 530.2 eV and 531.8 eV are attributed to Ti – O and C = O bonds [48, 51].

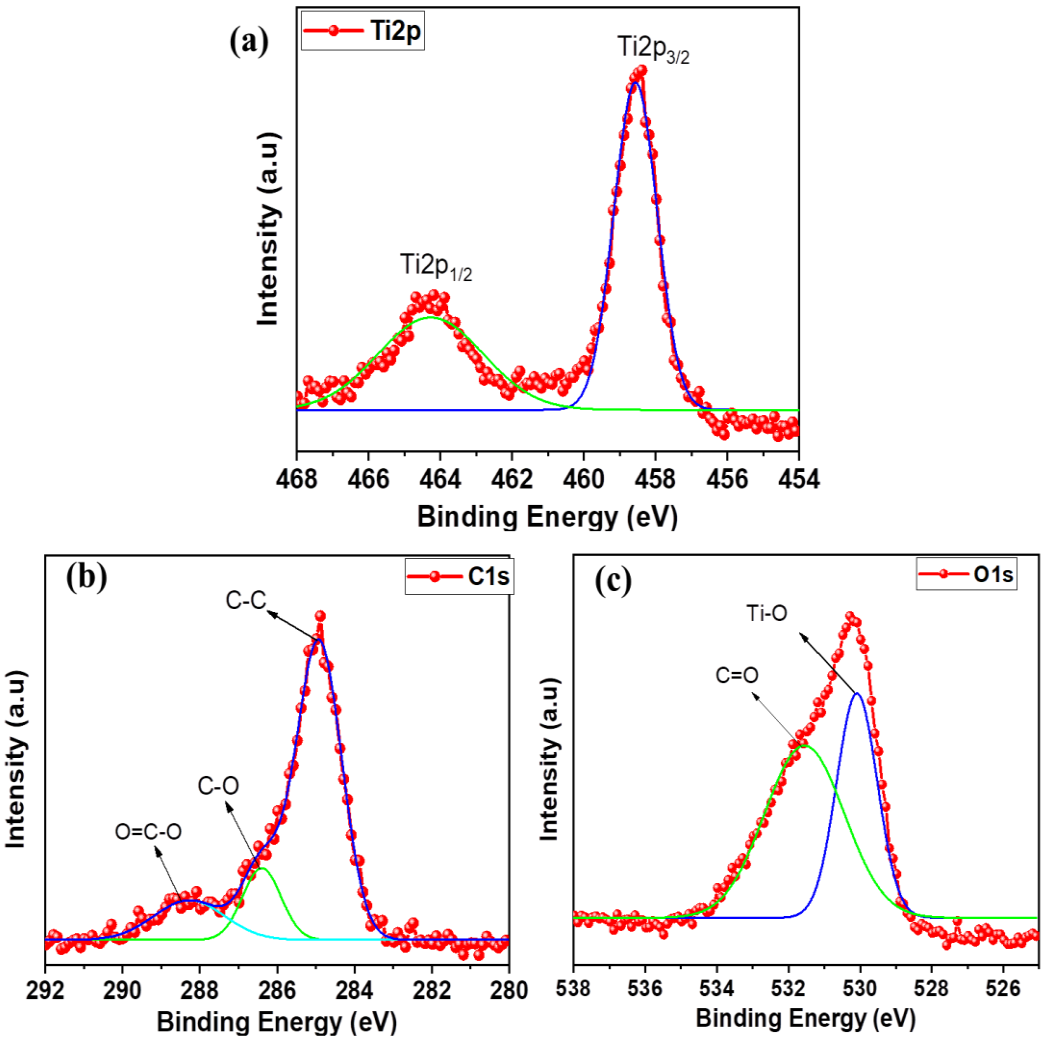


Figure 2.5: The XPS high resolution spectra of Ti2p (a), C1s (b) and O1s (c)

## 2.4.2 Particle Size Distribution Results

The particle size distributions of the milled powders are shown in Table 2.2. Additionally, Fig. 2.6 and 2.7 give the influence of milling speed and duration on average particle size of the powder achieved after grinding the chip. However, the vibratory disc mill demonstrated efficacy in reducing the size of Ti64 powder to a level suitable for commercialization in powder metallurgy. The particle size of Ti64 powders was detected to decrease as the milling speed and duration of the disc mill were increased.

Table 2.2: Particle size analysis with distribution size (d10, d50 and d90) of milled powders at variable milling speed, milling duration and atmosphere

| Sample | d10 (µm) | d50 (µm) | d90 (µm) | Specific Surface Area ($m^2$/kg) |
|---|---|---|---|---|
| DAT1330 | 46.4 | 142 | 269 | 16.73 |
| DAT1345 | 25.2 | 106 | 227 | 30.56 |
| DAT1360 | 18.2 | 90.2 | 202 | 39.13 |
| DAT1530 | 31.8 | 113 | 234 | 22.86 |
| DAT1545 | 19.8 | 97.6 | 209 | 36.46 |
| DAT1560 | 8.68 | 70.6 | 175 | 70.59 |
| DAR1330 | 52.7 | 142 | 272 | 14.25 |
| DAR1345 | 48 | 132 | 251 | 16.07 |
| DAR1360 | 49.1 | 127 | 236 | 15.90 |
| DAR1530 | 50.2 | 130 | 245 | 15.19 |
| DAR1545 | 38.6 | 113 | 225 | 18.74 |
| DAR1560 | 35.7 | 105 | 207 | 20.79 |

A minimum mean particle size of 70.6 µm was obtained for powders that were milled at 1500 rpm speed for a 60 min milling duration in air atmosphere. When compared to the DAR-coded samples, the mean particle size distribution of the DAT-coded samples is lower. It is known that oxygen has a negative effect on the ductility, fatigue strength, and stress corrosion of titanium alloys. Titanium alloys lose ductility with increasing oxygen content [52]. The absorption of impact energies by the Ti64 chip decreased with increasing oxygen content, as the oxygen in the air reacted with titanium, causing it to be more brittle and easily milled. Fine titanium powder is highly reactive overall and may easily react with oxygen and nitrogen in the atmosphere [53, 54]. The Ti64 powder containing high levels of O or N is brittle, resulting in reduced particle size as a result of milling. Argon gas was used to prevent titanium from reacting with oxygen and nitrogen.

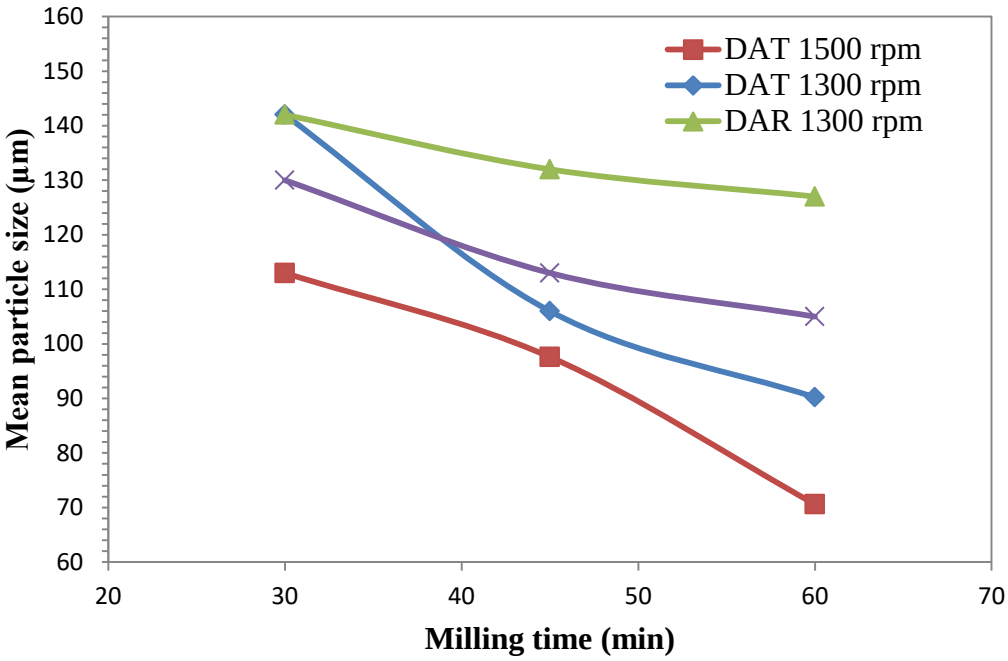


Figure 2.6: Mean particle size - milling duration graph of the Ti64 powders: Variation of d50 values with milling duration for different milling speeds

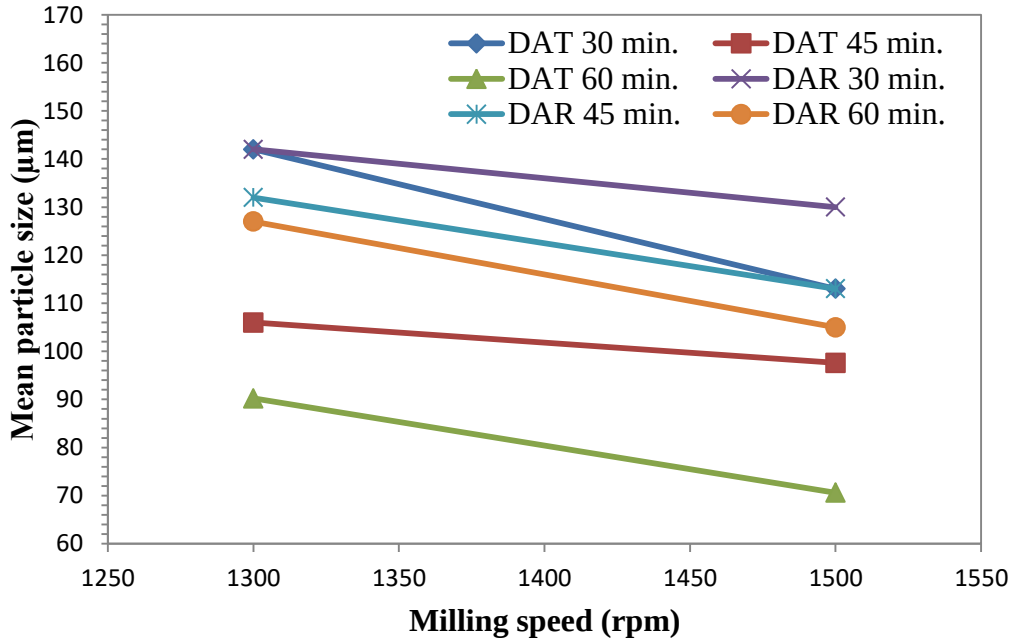


Figure 2.7: Mean particle size - milling speed graph of the Ti64 powders: Variation of d50 values with milling speed for different milling durations

### 2.4.3 The Crystal Structure Results

The XRD pattern of the Ti64 chip is given in Fig. 2.8. The XRD patterns for all samples revealed peaks of the phases α (hexagonal compact) and β (body centered cubic), which differed mainly in terms of the phases' peak intensity and number, as

confirmed by the micrographs [55]. Between 38° and 41°, the peaks can occur as a hexagonal structure for the planes α(002) and α(101) and form a cubic structure for the plane β(110). The hcp structure is also textured on the (100) and (102) planes [56]. It was observed peak intensity rose at the plane α(100). After milling, the intensity of X-ray beam and broadening of α(002) are reduced in comparison to α(101).

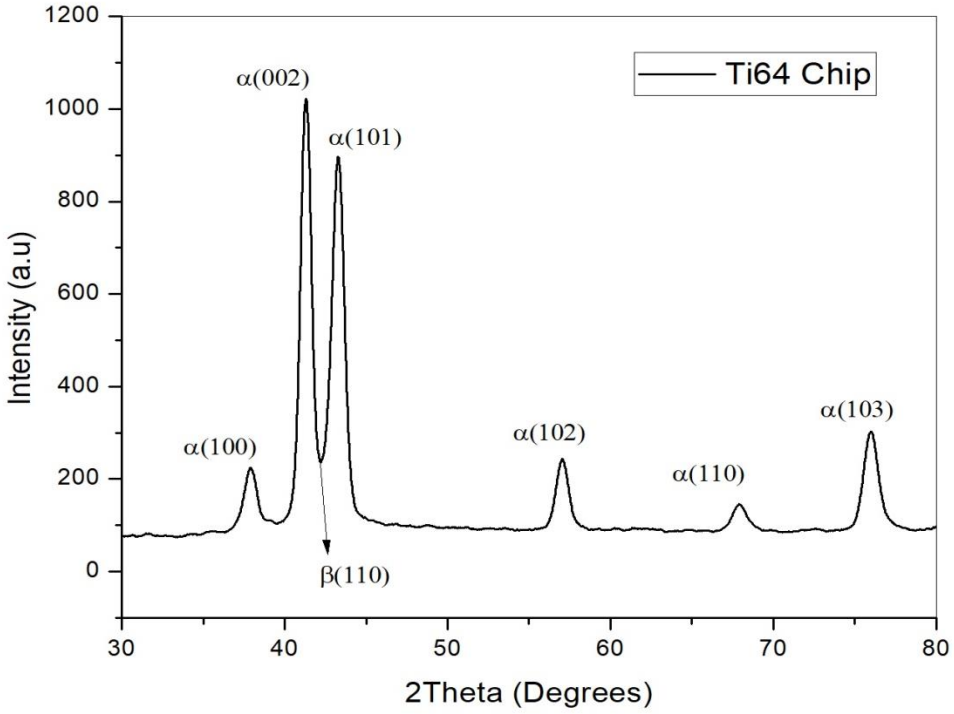


Figure 2.8: The XRD pattern of starting Ti64 chip

The XRD patterns of DAT-coded powders after milling in an air atmosphere are given in Fig. 2.9. The milling process decreases the intensity of the peaks of DAT-coded powders compared to the chip. As illustrated in Fig. 2.9, the intensity of diffracted peaks is affected by an increase in milling duration and speed. Deformation rate increases with an increase in milling duration and speed. This phenomenon is assumed to be a manifestation of crystal habit, and some intriguing correlations between morphology (crystal shape, particle size, and aspect ratio) and XRD peak intensity may occur [57]. After milling process, some new peaks appeared at 2θ values of 37 and 43°. Peaks at 37° and 43° indicate the presence of oxygen [58, 59]. As the milling speed and duration increase, the peak intensity at 37° and 43° increases. In the milling process, as the particle size decreases, the total surface area will increase, so the oxygen ratio in the powders increases. This also increases the

intensity of the oxygen-containing peak. The milling duration is an important parameter that determines the oxygen ratio of the powders. Although the peak intensities at 37° and 43° in DAT1330 and DAT1530 samples are similar, it is observed that the peak intensities increase as the milling duration increases.

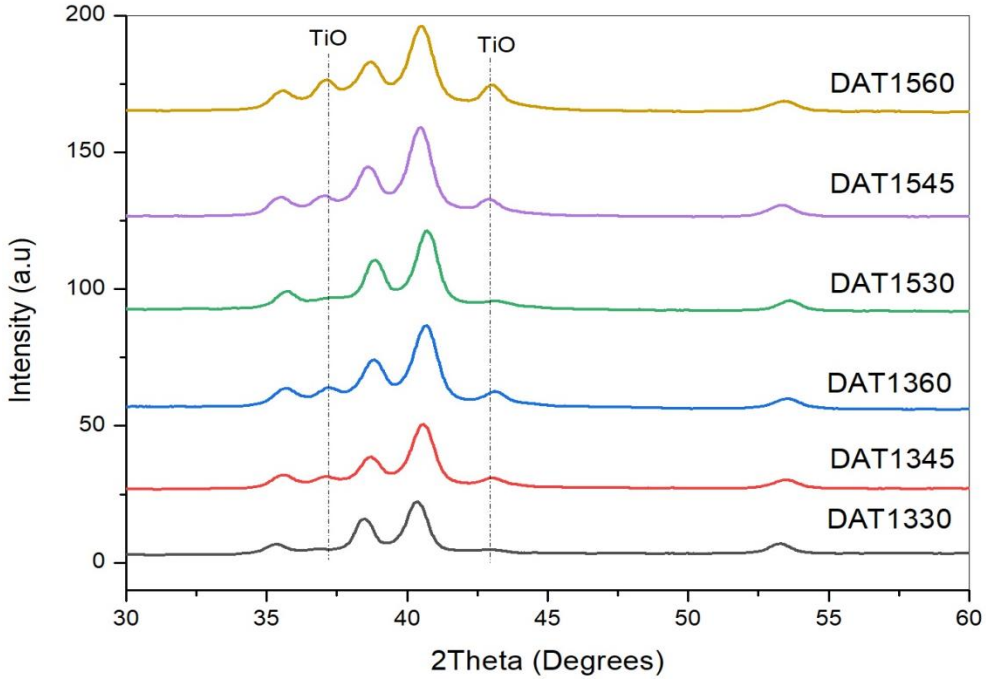


Figure 2.9: The X-ray pattern of DAT-coded Ti64 powders

Fig. 2.10 illustrates the XRD patterns of DAR-coded powders ground in an argon atmosphere. Despite the similarity between the patterns of the DAR-coded samples and the chip, a clear divergence has been observed within the stated range of 2θ. The XRD patterns of the chip and DAR-coded samples exhibit similar diffraction patterns. However, the peak intensities of DAR-coded samples are slightly higher than those of the chip and DAT-coded samples. It can be noticed in Fig. 2.9 and 2.10 that an increase in the deformation rate influences the x-ray intensity of the diffraction peaks [44]. Apart from the characteristic peaks, two different peaks are observed at 34° and 36°. Even if the milling process took place in an argon atmosphere, the presence of oxygen is observed. No significant change was observed in the intensity of these peaks with the milling duration and speed. The presence of oxygen in the Ti64 chip, which is the starting material, is also indicated in the XPS analysis.

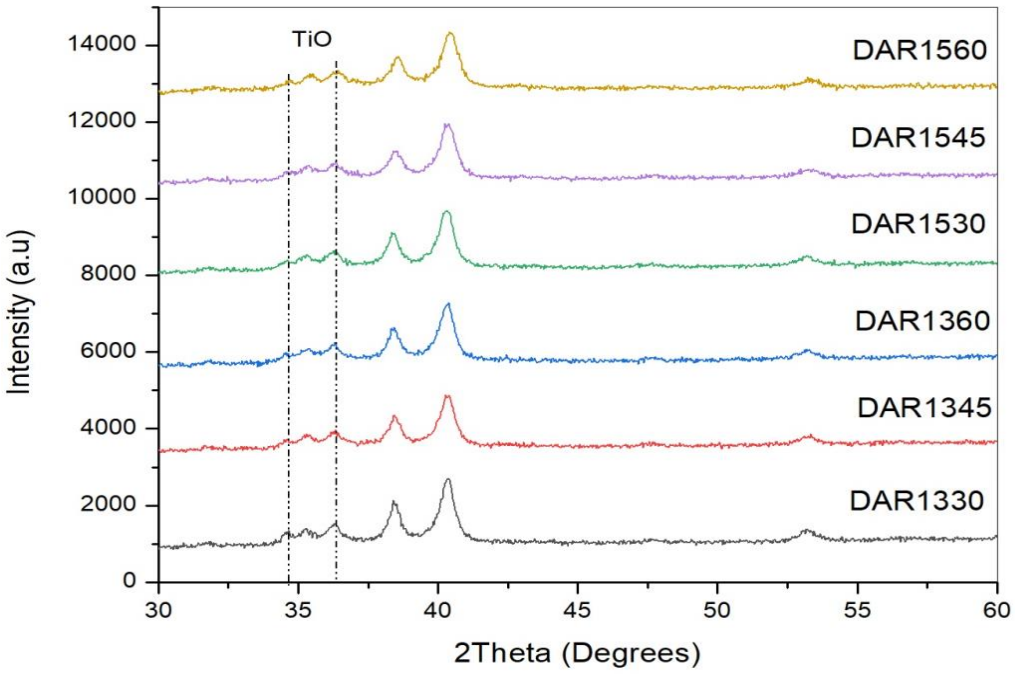


Figure 2.10: The X-ray pattern of DAR-coded Ti64 powders

Fig. 2.11 depicts the change in average crystallite size according to the milling duration and speed. Calculations of the average crystallite sizes of DAT- and DAR-coded samples were performed individually for dominant peaks. The curves indicate that the average crystallite size decreases as the milling speed and duration increase for all powder samples. The milling speed has a significant impact on powder size reduction. Compression and impact cause the particles to be stressed, resulting in size reduction. The impact energy on the particles increases as the milling speed increases. As the milling duration and speed increase, the increasing kinetic energy of the particles causes a decrease in the crystallite size [44].

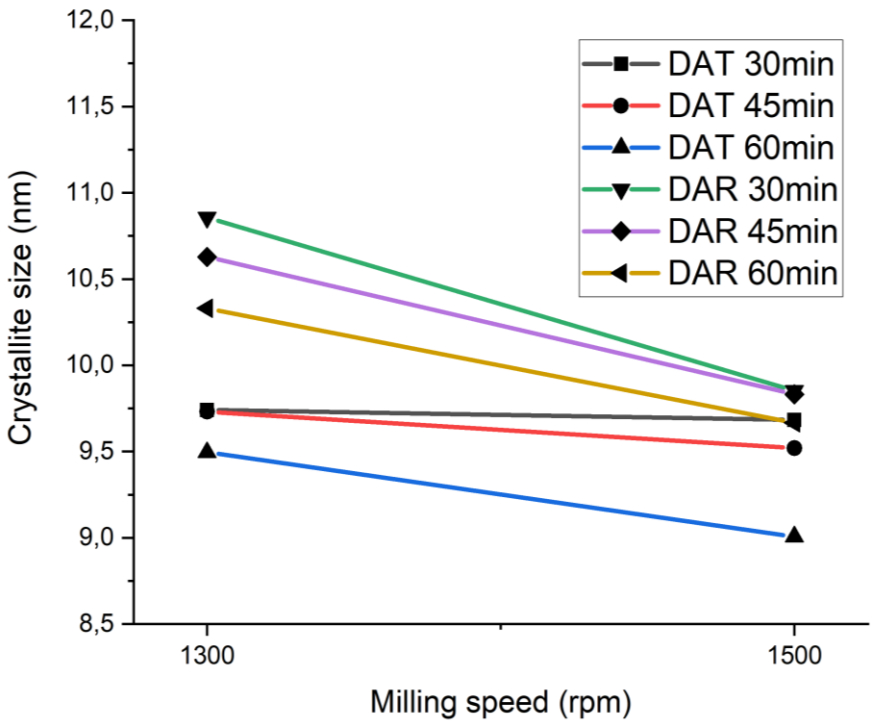


Figure 2.11: Differences in the average crystallite size of the Ti64 powders depend on the milling speed and duration

Tables 2.3 and 2.4 characterize the crystallite sizes of the DAT-coded and DAR-coded powders on the diffraction peaks of the α-Ti (101) phase. As previously stated, as the milling duration and speed are increased, the impact energy applied to the material increases and the mean particle size decreases. The results demonstrated that as the average particle size decreases, the powder crystal size decreases due to the large surface area of the powder. The difference in crystallite sizes between the DAT-coded and DAR-coded powders on the diffraction peaks of α-Ti is evaluated as the result of the difference in mean particle size. Another parameter to consider is temperature. Increasing the temperature of the grinding jar causes the powders to cold weld. The fact that the crystallite size of the powder decreases with increasing milling duration indicates that there is no cold welding. Cold welding of the powder particles is prevented by maintaining a constant temperature in the milling jar [39].

Table 2.3: The crystallite sizes of the DAT-coded powder on the diffraction peaks of α-Ti (101)

| **Sample** | DAT1330 | DAT1345 | DAT1360 | DAT1530 | DAT1545 | DAT1560 |
|---|---|---|---|---|---|---|
| **Crystallite size (nm)** | 10.65 | 9.95 | 9.86 | 10.29 | 9.80 | 9.47 |

Table 2.4: The crystallite sizes of the DAR-coded powder on the diffraction peaks of α-Ti (101)

| **Sample** | DAR1330 | DAR1345 | DAR1360 | DAR1530 | DAR1545 | DAR1560 |
|---|---|---|---|---|---|---|
| **Crystallite size (nm)** | 11.31 | 11.27 | 10.72 | 11.17 | 10.63 | 10.30 |

### 2.4.4 Morphology of the Powders

Fig. 2.12 displays the morphology of the DAT-coded powders at 500X and 1000X magnification. The influence of milling duration and speed on powder morphology is seen in Fig. 2.12. SEM images illustrate agglomeration and the forging effect. The powder is shown to have irregular and inhomogeneous particle morphologies. The powder particles were rubbed against the pot walls and discs in the vibratory disc mill. The powder size decreases with increasing milling duration and speed. The SEM results, on the other hand, demonstrate that the particles are agglomerated. As in Fig. 2.13, powder defects such as micro-cracks and nanoparticles (groups of small particles attached to the surface of larger particles) are observed [60].

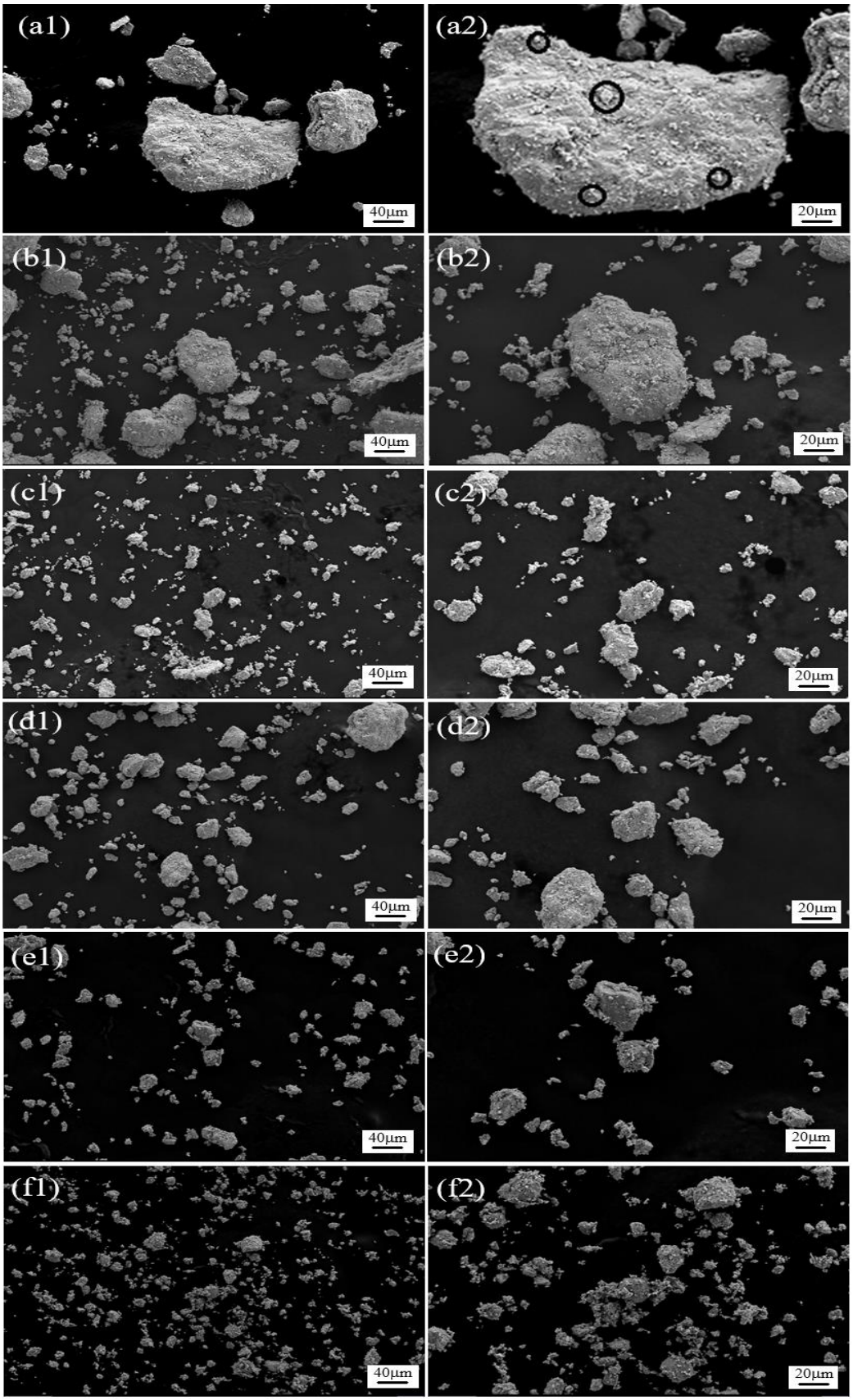


Figure 2.12: SEM micrographs of DAT-coded powders at 500x (1) and 1000x (2) magnification: DAT1330 (a1-a2), DAT1345 (b1-b2), DAT1360 (c1- c2), DAT1530 (d1-d2), DAT1545 (e1-e2), DAT1560 (f1-f2)

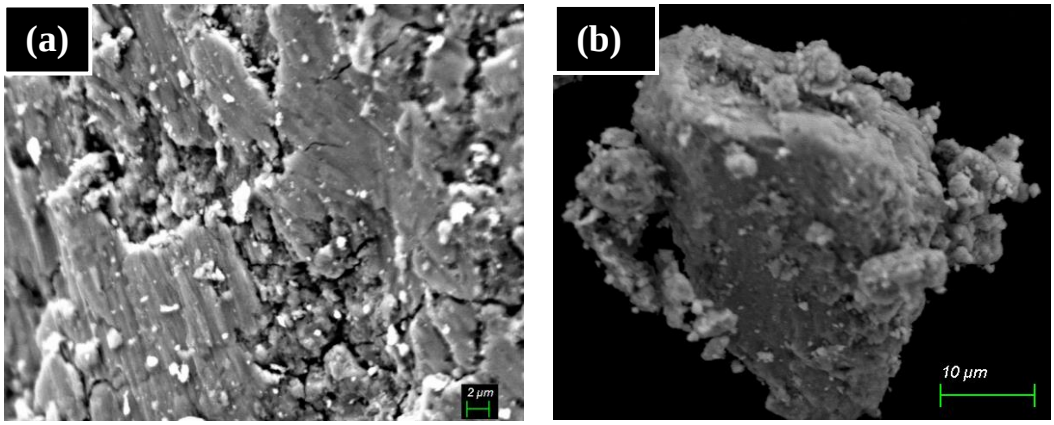


Figure 2.13: Powder defects; micro-cracks (a) and nanoparticles attached to the surface of larger particle (b)

SEM images of the DAR-coded powders are given in Fig. 2.14. It appears from the micrographs that the morphology of the powders is affected by the milling atmosphere. The powder morphology of the DAR-coded powders is more rounded than that of the DAT-coded powders. Unlike the DAT-coded powders, nanoparticles were not observed on the DAR-coded powders' surfaces. As milling duration and speed increase, the particle deviates from the leafy shape. The powder morphology changed from leafy to angular as milling duration and speed increased as given in Fig. 2.14 (f1-f2). Particle morphology includes a significant effect on powder flow rate. The flow rate analysis corroborated this conclusion as well.

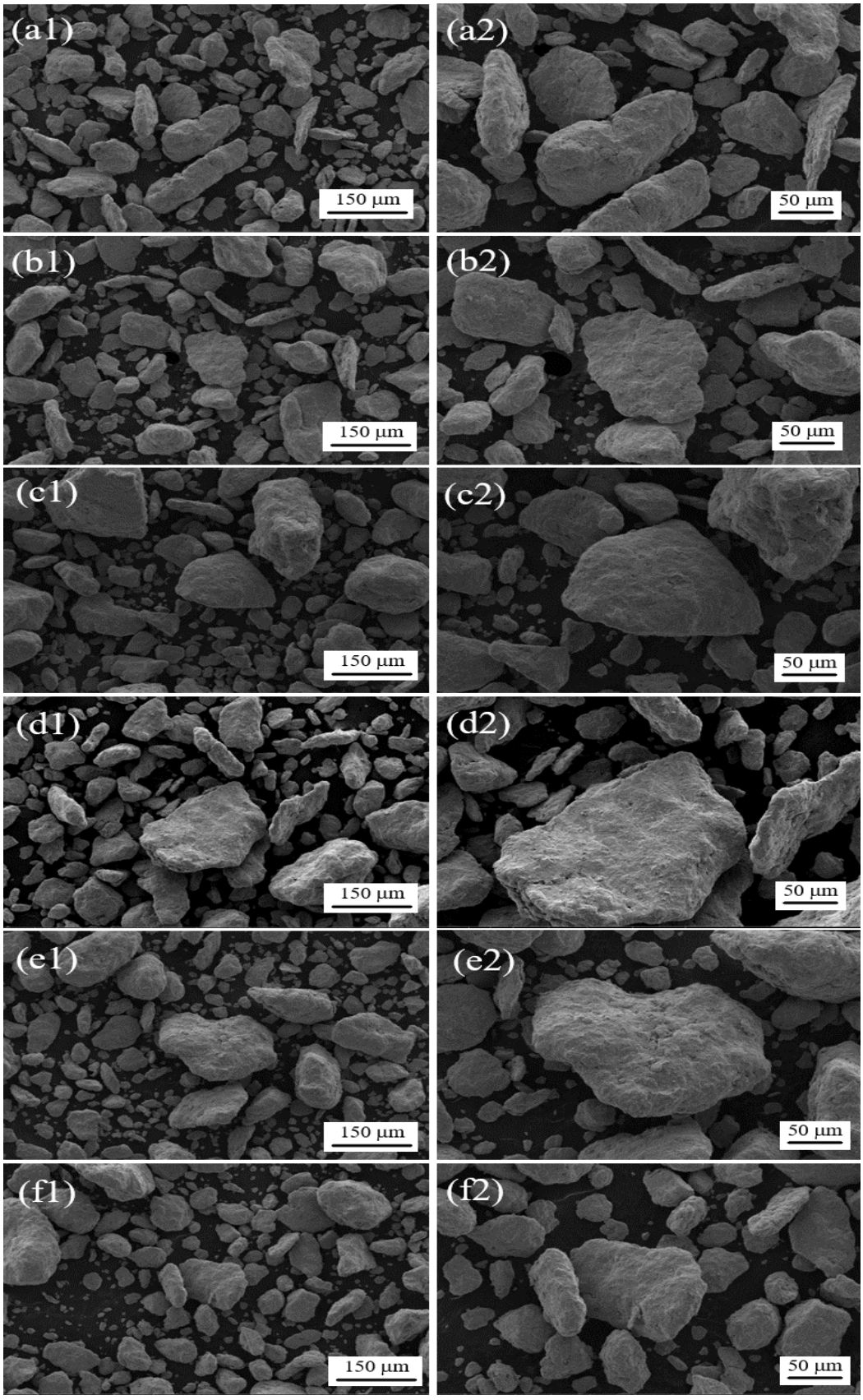


Figure 2.14: SEM images of DAR-coded powders at 500x (1), 1000x (2) magnification: DAR1330 (a1-a2), DAR1345 (b1-b2), DAR1360 (c1-c2), DAR1530 (d1-d2), DAR1545 (e1-e2), DAR1560 (f1-f2)

The Energy Dispersive X-ray (EDX) analysis was performed to determine the surface composition of the DAT-coded and DAR-coded powders. The related results are displayed in Table 2.5. It demonstrates that the contents of nitrogen (N) and oxygen (O) increased with increasing milling duration and rotation speed. The increase in oxygen content is due to the milling atmosphere and the increased particle surface area (particle size is decreased). The increase in nitrogen content, however, is attributable to surface contamination of the starting chip and the jar's temperature. The temperature of the jar increases as the rotation speed increases. Impurities were purged from the milling jar during the milling process using argon gas. When EDX results from the DAR-coded samples are compared to those from the DAT-coded samples a decrease in carbon and nitrogen levels is observed. No significant variations in oxygen levels have been detected in the DAR-coded samples. Accordingly, the optimal results were obtained with samples coded DAR1330 and DAR1560. Titanium is characterized by its tendency for oxygen and nitrogen absorption. The results conform to the literature findings [61, 62] that vibratory disc milling of Ti64 in an air atmosphere resulted in a significant O and N uptake. Although the milling was carried out in an argon atmosphere, the high oxygen content was observed.

Table 2.5: Surface composition with EDX analysis of the DAR-coded and DAT-coded powders

| | **1330** | | **1345** | | **1360** | | **1530** | | **1545** | | **1560** | |
|---|---|---|---|---|---|---|---|---|---|---|---|---|
| | **DAT** | **DAR** | **DAT** | **DAR** | **DAT** | **DAR** | **DAT** | **DAR** | **DAT** | **DAR** | **DAT** | **DAR** |
| **C** | 1.95 | 1.08 | 3.44 | 1.87 | 2.58 | 1.51 | 2.36 | 1.78 | 3.19 | 1.67 | 1.7 | 1.47 |
| **O** | 10.35 | 6.08 | 5.12 | 12.12 | 13.99 | 11.65 | 10.84 | 11.36 | 9.34 | 11.35 | 12.21 | 8.28 |
| **Al** | 5.49 | 4.06 | 1.92 | 5.63 | 5.94 | 4.94 | 5.37 | 6.08 | 3.72 | 5.14 | 5.02 | 5.39 |
| **Ti** | 76.23 | 85.10 | 85.06 | 77.72 | 76.04 | 78.86 | 70.38 | 77.65 | 74.93 | 79.05 | 70.42 | 81.88 |
| **V** | 4.43 | 3.15 | 4.01 | 2.40 | 4 | 2.93 | 3.98 | 3.10 | 4.02 | 2.50 | 4.02 | 2.88 |
| **N** | 0.00 | 0.00 | 0.00 | 0.00 | 0.00 | 0.00 | 5.93 | 0.00 | 3.34 | 0.00 | 5.47 | 0.00 |

### 2.4.5 Flow Characteristics and Bulk Density

The results of the ground powder flow rate test are given in Table 2.6. The flow rate of powders is attached to several physical properties (particle size distribution, alloy density, particle shape, surface morphology, and humidity) of the powder [63, 64].

Particle size has a significant effect on powder flowability. As particle size decreases, the surface area per unit mass of powder increases, leading to reduced flowability [65]. More contact surface area is available for cohesive forces in particular, as well as frictional forces that cause resistance to flow. Particle shape (aspect ratio) also has an effect on powder flowability. It influences the surface interactions between particles [66]. 50 grams of powder was used to experiment in the powder flow rate analysis. However, the DAT1345-DAT1360-DAT1545-DAT1560-coded powders had no flow rate because of the larger surface areas in contact with each powder. It has been reported in previous studies that a decrease in particle size causes a decrease in powder flow rate. Smaller particles have a high number of contact points with neighboring particles while large particles have fewer. Moreover, higher interparticle forces or mechanical interlocking enhance particles' cohesion between each other, resulting in reduced flowability [67, 68]. In the DAR-coded powders, although the particle size decreases, the powder flow rate increases due to their rounded corners and homogeneous morphological structure, as illustrated in Fig. 2.10. The flow rate of the DAR1330-coded sample was higher compared to that of the DAT1330-coded sample despite having the same mean particle size (d50). Similarly, when the DAR1560 (d50: 105 μm) and DAT1345 (d50: 106 μm) samples were compared, the former had 42.1 s/50g while the latter had no flow. This is most likely due to the presence of fine agglomerates and nanoparticles attached to the surface of larger particle within the powder, which increase inter-particle friction and reduce the powder's flow rate. This can be attributed to the irregular shape and interlocking of the particles, as well as the roughness of their surfaces [69].

Table 2.6: Flow rate and bulk density of the DAT-coded and DAR-coded powders

| | **Flow rate (s/50g)** | | **Bulk density (g/cm$^3$)** | |
|---|---|---|---|---|
| **Sample codes** | DAT | DAR | DAT | DAR |
| **1330** | 55.80 | 49.19 | 1.92 | 2.06 |
| **1345** | No flow | 48.33 | 2.08 | 2.18 |
| **1360** | No flow | 45.62 | 2.11 | 2.21 |
| **1530** | 59.68 | 45.17 | 2.15 | 2.18 |
| **1545** | No flow | 45.28 | 2.18 | 2.25 |
| **1560** | No flow | 42.10 | 1.97 | 2.31 |

Table 2.6 also displays the bulk densities of the powders. The bulk density of the powder is also referred to as its bulk density. Bulk density is defined as the weight of

a unit volume of powder and includes both the volume of its solid particles and the pores between them [70]. The bulk density of powders is determined by a variety of factors such as particle size, shape, surface roughness and particle size distribution. The bulk density analysis results indicate that all parameters have an effect on the bulk density of ground powders. When the same milling duration and speed parameters are used, the bulk density of DAT-coded powders was lower than that of the DAR-coded powders. This can be attributed to the lower average particle size distribution and more irregular particle shape of the DAT-coded powders. In general, the bulk density of a metal powder decreases with decreasing particle size [71, 72]. With the exception of DAT1560, the bulk density of the DAT- and DAR-coded powders increased as the particle size decreased. This can be because as the milling duration and speed increase, particle morphology becomes more regular and the surface roughness decreases. The lowest bulk density is found in the DAT1560 powder may be the result of finer particles, more irregular particle morphology, and heavily agglomerated and increased surface roughness. These results are consistent with the SEM analysis.

## 2.5 Conclusions

In this chapter, the particle size of Ti64powders was significantly decreased after performing a suitable vibratory milling process. The increase in milling speed and duration parameters resulted in a decrease in particle size. Additionally, the milling atmosphere (argon or air) has a direct effect on the particle size and morphology. When compared to the DAR-coded samples, the mean particle size distribution of the DAT-coded samples was lower. These differences can be explained by the impact energies produced when oxygen reacts with titanium. The impact energies absorbed by the Ti64 chip increased in the DAR-coded samples and decreased in the DAT-coded samples. Oxygen reacts with titanium, causing the samples to become more brittle and easily milled. Agglomeration and small particles attached to the surface of larger particles are observed during the milling process in an air atmosphere. In addition, the particle morphologies of the DAR powders were more rounded as a result of the milling process taking place in an argon atmosphere. As the milling duration and speed increased, the crystallite size of the powders decreased in proportion to the mean particle size. The difference in the crystallite sizes between

the DAT and DAR powders is evaluated as a result of the difference in mean particle size. Although the particle size of the DAR-coded powders decreased, their flow rate increased due to their rounded corners. Due to their more irregular shape, the presence of nanoparticles on large particles, and the interlocking of the particles, the DAT-coded samples exhibited poor flow rate or no flow at all. The particles' morphology and size distribution have a significant effect on the bulk density. The bulk density of DAT-coded powders is lower than that of the DAR-coded powders because of the DAT-coded powders' more irregular particle morphology and lower average particle size characteristics.

# Chapter 3

# The Use of Titanium Chip for Epoxy Composites via Circular Economy Approach

## 3.1 Introduction

A composite is a result of combining at least two distinct components to manufacture a novel engineering material with enhanced qualities. The matrix and reinforcements are the two fundamental constituents of composite materials. It can be categorized in polymer, metal, and ceramic according to the matrix type. The primary advantages of composite materials over metal and ceramic materials are their high strength and stiffness, combined with low density compared with bulk materials, allowing for a weight reduction in the finished part [1, 73, 74].

The two most prevalent types of polymers are thermosets and thermoplastics. Thermoplastic polymers have little to no reticulation, are often solvent soluble, and melt readily. Thermosetting polymers or thermosets are heavily cross-linked, solvent-insoluble, and infusible. Today, polypropylene (PP), polyvinyl chloride (PVC), polylactic acid (PLA), polystyrene (PS) and polyethylene (PE) can be counted as the most widely used thermoplastics. Epoxy, polyester and elastomer (natural rubber) are typical examples of thermosets [75, 76]. In polymer matrix composites, thermoset polymers have been of significant importance [77]. Epoxy is a commonly used polymer in multiple applications ranging from coatings, corrosion protectants, flooring, electrical and electronic instruments, sports equipment, and many more. In automotive applications, epoxy-based coatings prevent rust and

corrosion. The major advantage of polymer composites over metallic materials is their ease of processing, productivity, cost reduction, high strength, modulus-weight ratio, etc.

Typically, the reinforcement consists of a fiber or a particulate. The two sub-categories of particle-reinforced composites are large-particle and dispersion-strengthened composites. The distinction between these is determined by the reinforcement or strengthening mechanism. The particulate component of the majority of these composites is tougher and stiffer than the matrix [4, 5]. Numerous metallic powders and particles have been used as reinforcement materials for polymeric composites. Metals as fillers for polymer composites have attracted the interest of industry and the research community primarily because such a composite enables the extraction of the best properties from two materials with diametrically opposite functionality [78]. Particulate fillers are utilized to modify the physical and mechanical properties of polymers in various ways. To adjust the creep, impact, thermal, electrical, and magnetic properties of polymer composites, reinforcements such as metal flakes, and metal powder are typically utilized. The mechanical properties of the composites have been affected by the particle shape, size, and surface area of such additional particles [8, 9, 79].

In the power industry, inorganic fillers (such as aluminum nitride (AlN), boron nitride (BN), silica ($SiO_2$), alumina ($Al_2O_3$), titanium oxide ($TiO_2$), silicon carbide (SiC) and zinc oxide (ZnO), etc.) are generally added into polymers to attain certain electrical, mechanical, and thermal properties [80]. Epoxy-based composites have historically been utilized extensively in the power and microelectronics industries thanks to their superior mechanical, electrical, and thermal properties in conjunction with their economical and appropriate processability. Epoxy resin is known to be a widely used material for stator floor wall insulation systems in the energy industry. Epoxy resins containing micro-size inorganic reinforcements are especially applied for dry distribution transformers, voltage and current transformers [81]. Besides the thermal conductivity, and electrical properties, mechanical strength of polymer composites has a crucial role in specific applications. Epoxy composites with high mechanical strength are also used in the insulation systems of big electrical machines. For several applications in automotive, aircraft, and maritime industries, it

is preferred to use lightweight materials with increased mechanical strength [82]. Yamamoto et al. [83] examined that the structure and shape of silica particles had important influences on mechanical properties, including fatigue resistance, and tensile and fracture strength of the epoxy composite. Nakamura et al. [84] noted the consequences of the size and shape of silica particles on the strength and fracture toughness based on particle-matrix bonding and also reported an improvement in the flexural and tensile strength as the specific surface area of particles grew [85]. Moses et al. investigated the mechanical properties of epoxy resin reinforced with metal powders. According to their work, the tensile strength of epoxy filled with metal particles is shown to increase when compared to unfilled epoxy. The filling of a polymer with electrical conductive metallic particles increases both the electrical and thermal conductivity of the composites obtained, which seems to be the focus of the majority of research where metallic particles are used as reinforcements in polymer composites [16]. Tekçe et al. [86] pointed out the shape factor of fillers has a strong influence on the thermal conductivity of the composite. Reinforcements with a lower aspect ratio can develope certain mechanical properties [87]. Hussian et al. [88] stated that utilizing ceramic filler in epoxy composites results in enhanced physical, rheological, and thermal properties. Additionally, Young's modulus and flexural strength can be enhanced. Goyanes et al. [89] discussed for aluminum-epoxy composites that density increases with increasing filler content, again following the rule of mixture. A relation between Young's modulus and its density for filled epoxy composites was also proven by Tilbrook et al. [90].

In this study, recycled Ti64 powder and epoxy resin are used to generate particle-filled polymer composites. Mechanical properties, such as tensile strength, flexural strength, and microstructure of the specimens have been investigated. This research assessed the thermal stability of Ti64 powder reinforced epoxy with varying filler contents and particle size. The thermal measurement was performed via TGA in an inert environment (nitrogen gas). The influence of Ti64 powder content on the mass loss rate, degradation temperature, and residual mass were taken into account. The thermal conductivity of Ti64 powder-filled epoxy resin at various filler loadings was investigated. The thermal conductivities were measured and the effect of filler dispersion on thermal conductivity was examined.

## 3.2 Materials and Method

Ti64 alloy powder, obtained after mechanical milling, planned to be utilized as a reinforcement material in epoxy composites. Irregularly shaped Ti64 powder was utilized in this study.

The average particle size of the powders, with dispersion by a range of dry units, was obtained via a laser diffraction particle size analyzer (Malvern Mastersizer 3000). Two kinds of recycled Ti64 powder fillers with average particle sizes d(50) of 15.4 μm and 34.6 μm were used.

A commercially available epoxy Brv Sc 330 was used as the matrix material. The epoxy resin was used together with the slow hardener; both were acquired from Brv Epoksi (Izmir, Turkey), given in Table 3.1.

Table 3.1: Typical properties of the epoxy resin

| **Appearance** | **Transparent** |
|---|---|
| **Color** | Clear |
| **Density** | 1,10 g/cm³ |
| **Flash point** | >25 °C |
| **Mix ratio (weight)** | 5 / 3 |
| **Usable life** | 30 min / 25°C |
| **Cure time** | 12 hour / 25°C |

The epoxy was combined with the hardener in a ratio of 5:3 in accordance with the datasheet provided by the supplier. Four formulations ranging from 0, 3, 5 to 10 wt% Ti64 powder in epoxy were developed as summarized in Table 3.2. Ti64 particles with two different particle sizes were used to investigate the effect of particle size on final the properties of the polymer composites.

Table 3.2: Four formulations ranging from wt% Ti64 powder in epoxy were developed as summarized

| Sample code | Mean particle size (µm) | Epoxy (wt %) | Ti64 powder (wt %) |
|---|---|---|---|
| Neat | unfilled | 100 | 0 |
| A3 | 15.4 | 97 | 3 |
| A5 | 15.4 | 95 | 5 |
| A10 | 15.4 | 90 | 10 |
| B3 | 34.6 | 97 | 3 |
| B5 | 34.6 | 95 | 5 |
| B10 | 34.6 | 90 | 10 |

A specially designed and fabricated silicon mold is used for this purpose to avoid stick during curing, as shown in Fig. 3.1.

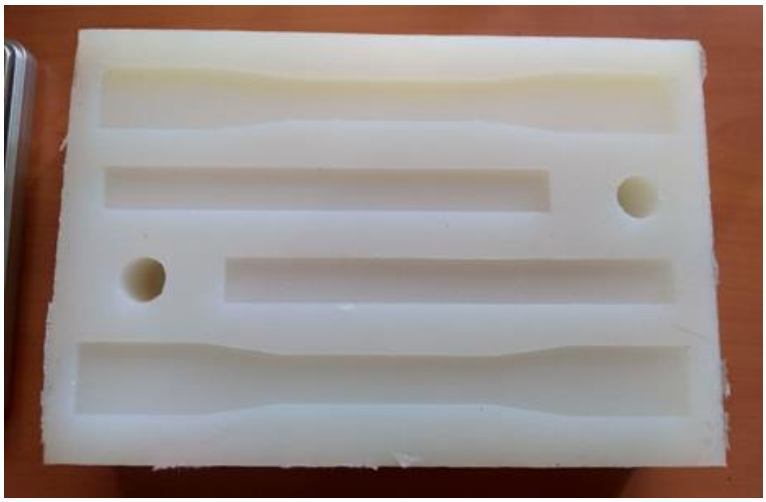

Figure 3.1: A specially designed and fabricated silicon mould

Ti64 powder was oven-dried for 24 h at 80 $^{o}$C. Ti64 powder was mechanically mixed with epoxy at a low speed stirred to avoid bubbles and hardener was mixed into the mixture of Ti64 powder/epoxy. Fig. 3.2 illustrates the production process of epoxy composites. In the case of particulate reinforced composites, Ti64 powder is added to the epoxy resin first and mixed well using a continuous stirring process before the hardener is added along with the Ti64/epoxy mixture. The duration of the mixture's stirring is determined by the exothermic reaction. The neat epoxy resin samples were likewise prepared under similar processing conditions, but without Ti64 powder.

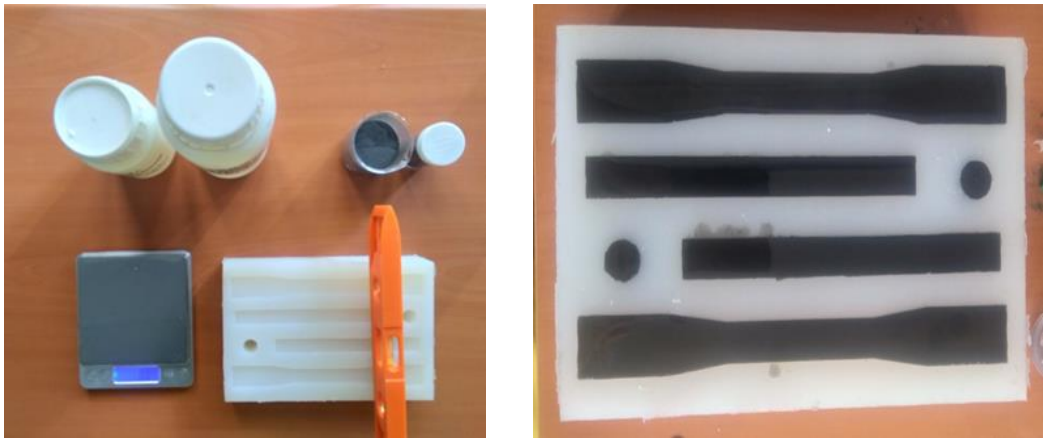

Figure 3.2: Production process of the epoxy composites

The three-point bending test was executed with a constant loading speed of 1.0 mm/min at room temperature, and a span length of 102.4 mm in accordance with ASTM D790 using a Shimadzu universal testing machine. The dimensions of the specimens are 125 mm × 12.7 mm × 3.2 mm with a span of 102.4 mm length as given in Fig. 3.3. The tests were conducted in the three point bend configuration in at a span to depth ratio of 32. The flexural modulus values were determined from the slope of a stress-strain curve produced by three-point bending test using a Shimadzu testing device.

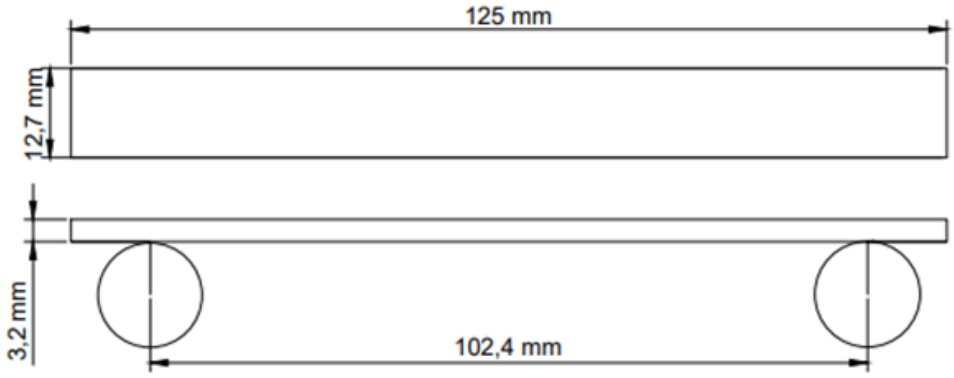


Figure 3.3: Dimensions of three point bending test specimen (ASTM D790)

Using the universal tensile strength testing machine Shimadzu (AG-IC 100kN), laboratory tests was conducted at a deformation rate of 1 mm/min at room temperature. Fig. 3.4 shows the dimensions of a tensile test specimen according to American Society for Testing and Materials (ASTM) D638-03 Type I. Based on the results from the Shimadzu (AG-IC 100kN) machine, the calculation of ultimate

tensile stress and Young's modulus of the composites were obtained from the following equations:

$$E = \frac{\sigma}{\varepsilon} \tag{2}$$

$$\sigma = \frac{F}{A} \tag{3}$$

$$\varepsilon = \frac{\Delta L}{L_0} \tag{4}$$

Where $E$ is the Young's modulus, $F$ is the maximum force, $A$ is the actual cross-sectional area of the specimen, $\Delta L$ is the amount by which the length of the object changes, $L_0$ is the original length of the object, $\sigma$ the applied tensile stress and $\varepsilon$ the longitudinal elastic deformation of the specimen.

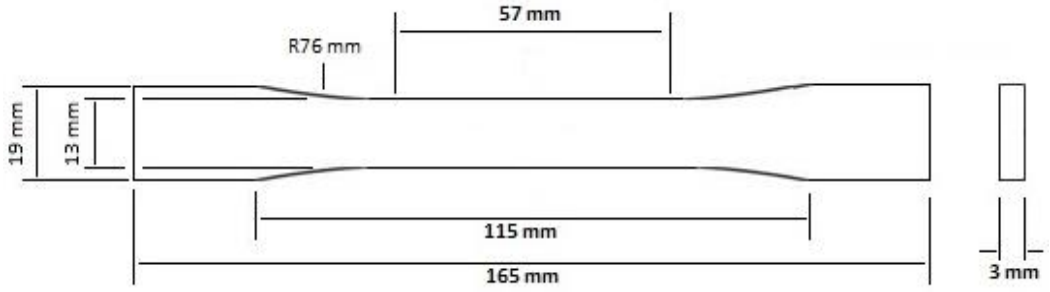


Figure 3.4: Dimensions of tensile test specimen (ASTM D638-03)

As shown in Fig. 3.5, thermal conductivity measurements were conducted using a C-Therm TCI test machine in accordance with ASTM D 5470. The cylindrical testing samples had a diameter of 20 mm and a height of 3 mm. The thermal conductivity of various proportions of Ti64 filled epoxy resin composites are determined.


Figure 3.5: C-Therm TCI test machine according to ASTM D 5470

To investigate the degradation behavior of the films in the presence of high temperatures, a thermogravimetric analysis was performed. A Netzsch STA 449 F3 Jupiter Thermal Analyzer was used to perform the measurements (Selb, Germany). All samples were heated at a rate of 10 °C/min from 20 to 900 °C. Initial degradation temperatures were calculated using extrapolated onset temperatures in accordance with ISO 11358-1.

## 3.3 Results and Discussion

### 3.3.1 Characterization of the Recycled Ti6Al4V Powder

Three specimens of each type were tested. The results of the three tests were averaged. Neat and Ti64 powder-reinforced epoxy composites produced at variable filler content by weight were observed to have no visible defects or other issues. The average particle size data of the powders were obtained from 50 g powder. Particle size and size distribution data can be expressed either tabularly or graphically. Table 3.3 summarizes the particle size data extracted from the laser diffraction particle size measurement. The specific surface area values given by the particle size measuring device was also added to the table. In addition, the amount of oxygen and nitrogen contained in the powders is given in Table 3.3. It is observed that the concentration of oxygen increases as the particle size decreases. It is stated in the literature that the concentration of oxygen in the chemical composition of the powder determines the

characteristic of the matrix-particle interface. LECO TC400 instrument was used to determine oxygen in powders A and B with different size distribution. The LECO TC400-Series instrument identifies nitrogen/oxygen in metals, refractories and inorganic materials using the basis of inert gas fusion.

Table 3.3: Summarizes the recycled Ti6Al4V powder characterization

| Ti64 Powder | d(10) µm | d(50) µm | d(90) µm | Specific Surface Area ($m^2/kg$) | Oxygen (%) |
|---|---|---|---|---|---|
| **A** | 4.40 | 15.4 | 35.7 | 686.8 | 3.48 |
| **B** | 14.4 | 34.6 | 60.7 | 271.3 | 2.09 |

Based on the particle size data presented in Table 3.3, particle size distribution was plotted. Fig. 3.6 and Fig. 3.7 show number frequency histograms of two kinds of recycled Ti64 powder particle size data in linear scale, respectively.

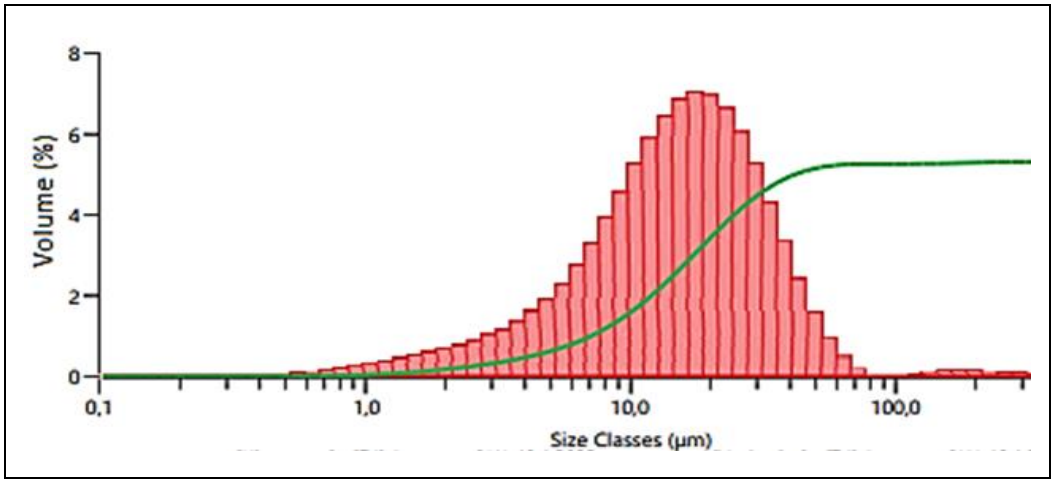


Figure 3.6: Histogram of recycled A powder particle size distribution

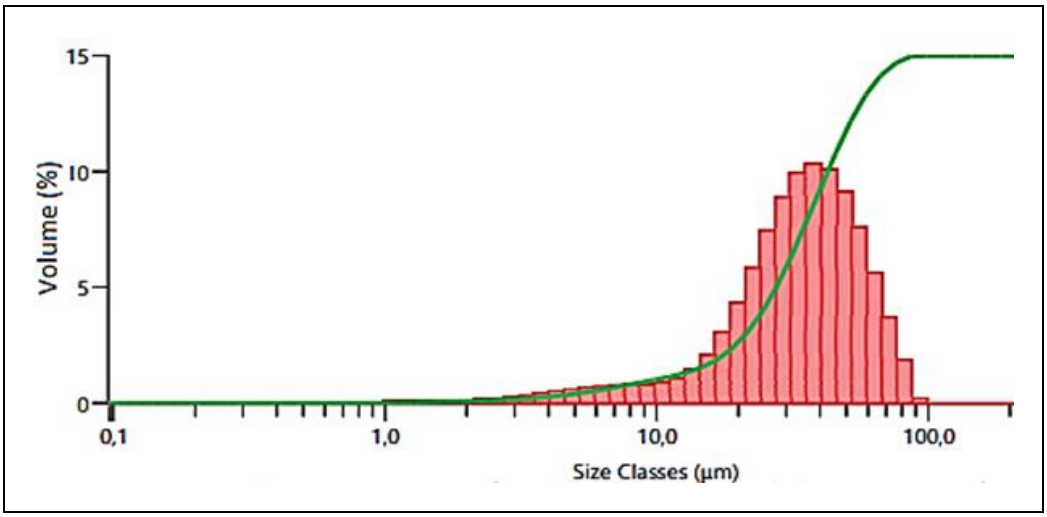


Figure 3.7: Histogram of recycled B powder particle size distribution

Figure 3.8 illustrates SEM images of the Ti64 powders: (A) - (B) powders and displays the morphology of the powders at 2.5 kX magnification. SEM images illustrate agglomeration and the forging effect. The powder is observed to have irregular and inhomogeneous particle morphologies with an elongated shape. As in Fig. 3.8, powder defects such as micro-cracks and nanoparticles (groups of small particles attached to the surface of larger particles) are observed.

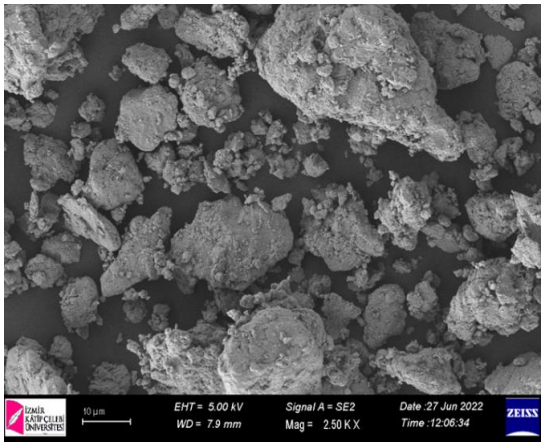


(A)

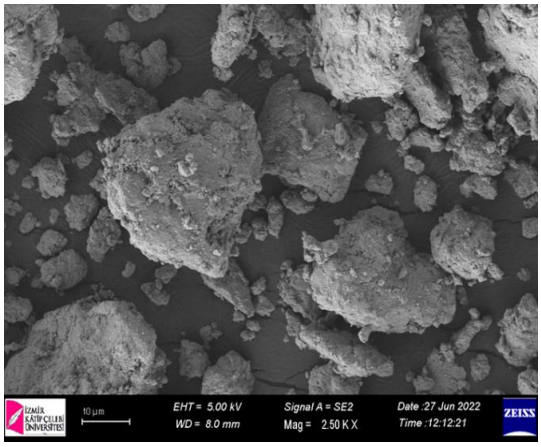


(B)

Figure 3.8: SEM images of the Ti64 powders: (A) and (B) powders

### 3.3.2 Tensile Strength Test of the Ti64 Powder Reinforced Epoxy Composites

All fractured regions of the composites are given in Fig. 3.9.

Figure 3.9: Fractured region of the epoxy composite samples after the tensile analysis

Tensile strength of the epoxy composites was found to increase with a decrease in particle size but with increased particle contents, as shown in Table 3.4 and Fig. 3.10. It was observed that there is considerable progress in tensile strength with increased filler ratio. This can be explained by the surface contact area effect. As stated in the literature, the surface contact area has a considerable impact on the mechanical properties of the polymer composites.

Table 3.4: Tensile strength results of the epoxy composites

| Sample | Tensile Strength ($N/mm^2$) | Young's Modulus (MPa) |
|---|---|---|
| Neat | 33.96 ±2.32 | 860.98 |
| A3 | 36.42 ±4.04 | 1184.96 |
| A5 | 40.86 ±3.23 | 1381.18 |
| A10 | 44.57 ±3.27 | 1461.62 |
| B3 | 35.09 ±4.29 | 897.07 |
| B5 | 38.14 ±3.62 | 1196.96 |
| B10 | 41.74 ±3.12 | 1381.77 |

Due to the increasing content of Ti64 powder fillers in the polymer structure, the total surface contact area of powder increases. Therefore, the tensile strengths of the

fabricated samples are increased significantly after incorporating of Ti64 reinforcing powder in the epoxy. However, it is stated in the powder characterization section that the surface contact area of powder A is higher than powder B. Therefore, when A and B reinforced epoxy composites are compared, the tensile strength of A composites is higher. In resin, the homogeneous dispersion of filler is crucial: the rise in surface area increases the tendency for the particles to agglomerate and such agglomerations can be arduous to separate. Marghalani [91] demonstrated in their investigations that the irregular form of the particles provided a good correlation between the polymer matrix and the reinforcement.

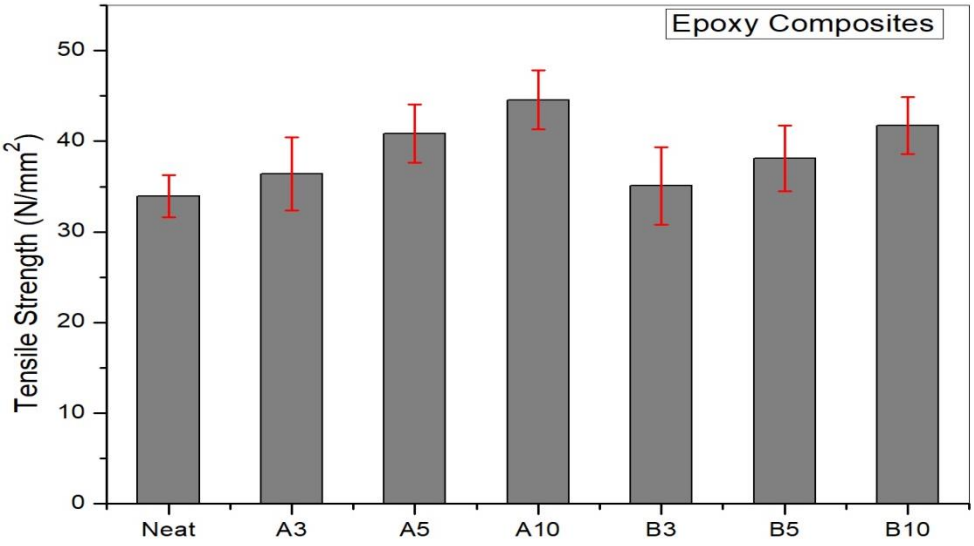


Figure 3.10: Tensile strength results of the epoxy composites

Wetting the filler with the matrix is crucial when incorporating the filler into the resin [92]. The results of the experiments confirmed that there was a fine increase in the adhesive bonding strength of the composites with the addition of the Ti64 microparticles. Thus, the hypothesis regarding the wetting of the filler with the matrix and the positive influence of the Ti64 powder filler on the tensile strength was confirmed. The research results confirmed a satisfactory wettability between the epoxy resin and the Ti64 powder filler.

Figure 3.11 shows the tensile stress -strain curves for neat epoxy and Ti64 powder reinforced epoxy composites. It can be noticed that the strain values decreases when added B powder to the epoxy resin. The elongation values was increased for A5-A10 samples but decreased for A3 sample. Particle size and particle-matrix interface bonding affected tensile properties of the composites[93, 94].

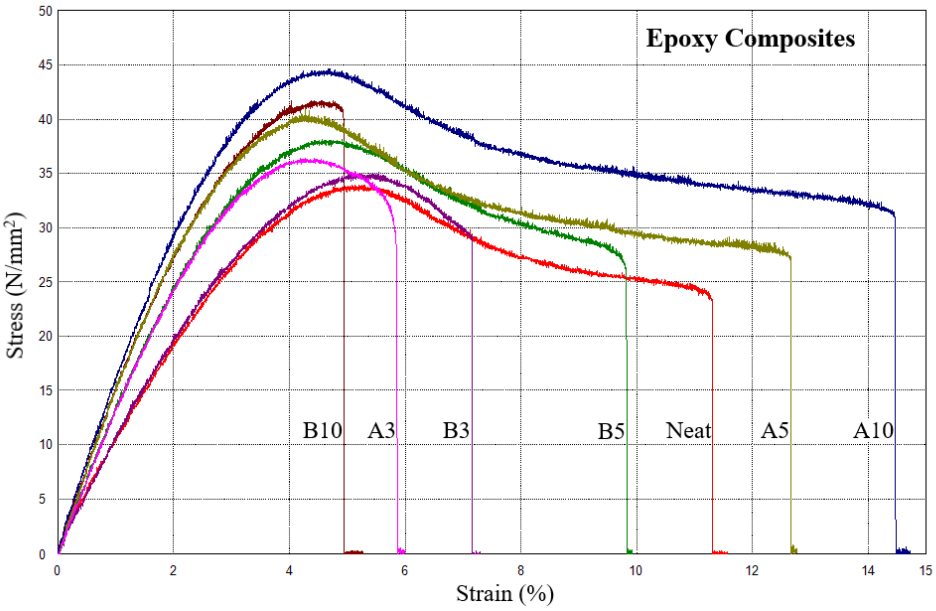


Figure 3.11: The stress-strain curves obtained in the tensile test of the epoxy composites

The findings of the tensile test indicate that there is a powerful interaction between the Ti64 powder as filler and the epoxy as matrix. The significant decrease in fracture strength of the composite with increasing filler volume fraction exhibits poor particle-matrix adhesion. However, the fact that the fracture strength remains approximately constant or increases with increasing volume fraction means that the particles are firmly bonded within the matrix [95].

However, the particle-matrix interfacial bonding has a significant effect on the strengthening mechanism. The particle-matrix adhesion also impacts the attitude of the composite. This situation can be explained by the distinction in the stress state around well or weakly bonded particles. Moreover, the stress transfer between the particles and the matrix largely determines the strength mechanism. For particles that strongly bonded to the matrix, the maximum stress can be effectually transferred from the matrix to the particles, which obviously increases the strength. The applied stress can be found above and below the poles of the particles. However, for weakly bonded particles, adding particles to the matrix results in a decrease in strength. A weakly bonded microparticle will act like a gap in the matrix [95-99].

### 3.3.3 Three Point Bending Test of the Ti64 Powder Reinforced Epoxy Composites

The measured flexural strength of the epoxy composites were performed using three-point bending analysis, in Fig. 3.12. The flexural strength tests were executed in the three-point bend arrangement in conformity with ASTM D790-07 at a span-to-depth ratio of 32.

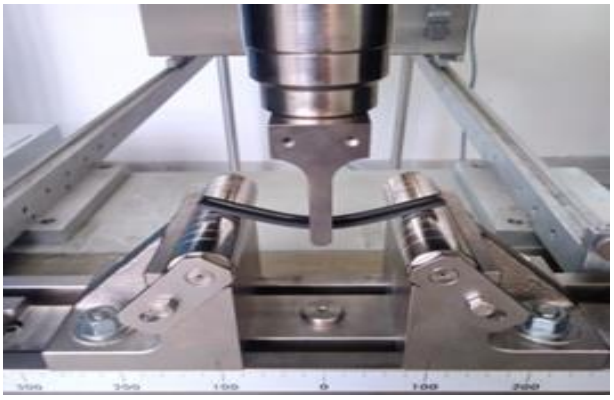

Figure 3.12: The three point bending testing machine

The microstructure of the composite and the interfacial bond between the reinforcement and the matrix determine the flexural strength and modulus of the composites [100]. Factors such as the amount of particle filler particle-matrix bond strength, and particle size determine the flexural strength of a particle-reinforced PMC [101]. As shown in Table 3.5 and Fig. 3.13, notable distinctions in flexural results were followed among composites with distinct filler sizes.

Table 3.5: Three point bending test results of the epoxy composites

| Sample | Flexural Strength ($N/mm^2$) | Flexural Modulus (GPa) |
|---|---|---|
| Neat | 63.71 ±2.51 | 1.223 |
| A3 | 78.49 ±4.18 | 1.833 |
| A5 | 80.22 ±3.10 | 1.944 |
| A10 | 86.58 ±3.26 | 2.408 |
| B3 | 71.96 ±4.45 | 1.522 |
| B5 | 78.13 ±3.41 | 1.667 |
| B10 | 84.37 ±3.55 | 1.773 |

The results revealed that the flexural strength increases with the larger filler loading. Additionally, the flexural strength of sample A is greater than that of sample B. This can be explained as follows: Smaller particles have higher-quality dispersion and a greater surface contact area within the matrix [98]. Consequently, the smallest Ti64 particle size provides superior flexural strength. Some important characteristics of composites should to be considered in order to explain this phenomenon. The quality of the interface in composites, i.e., the static adhesion strength and interfacial stiffness, usually play a crucial role in the ability of the materials to transfer stresses and elastic deformation from the matrix to the fillers [85].

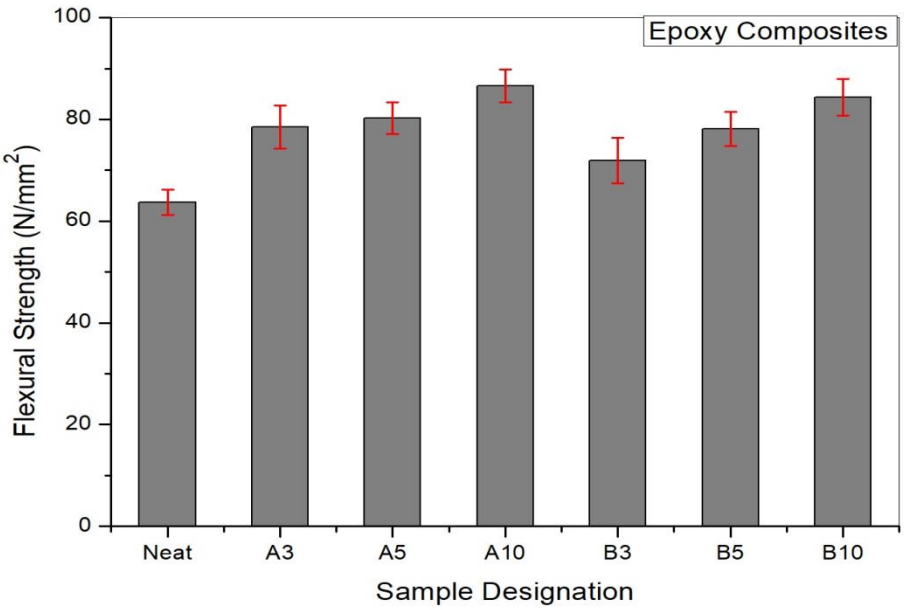


Figure 3.13: Three point bending test graph

### 3.3.4 Thermal Conductivity Test of the Ti64 Powder Reinforced Epoxy Composites

The experimental consequences of the thermal conductivity measurements of Ti64 powder reinforced epoxy composites are given in Table 3.6. Most of the used polymers are thermally insulating and have a thermal conductivity ranging from 0.1 to 0.5 W/mK [102]. In the literature, several studies have taken on experimentally determining the thermal conductivity of bulk Ti-6Al-4V. Researchers found it to be between 6.20 and 7.66 W/mK [103-105]. The thermal conductivity of a composite consisting of one type of filler added to a polymer matrix depends on the thermal

conductivity of the components, the morphology, size, and concentration of the fillers, their dispersion within the polymer, and the thermal interfacial resistance [8].

Table 3.6: The thermal conductivity results of the Ti64 powder-reinforced epoxy composites

| Sample | Thermal conductivity (W/mK) |
|---|---|
| Neat | 0.2438 ±0.08 |
| A3 | 0.2614 ±0.15 |
| A5 | 0.2869 ±0.23 |
| A10 | 0.2974 ±0.20 |
| B3 | 0.3083 ±0.11 |
| B5 | 0.3681 ±0.28 |
| B10 | 0.4792 ±0.19 |

The adding of the fillers to the epoxy matrix significantly raised the thermal conductivity of all the epoxy composites. The addition of Ti64 powder to the epoxy resin considerably increased the thermal conductivity of the composite compared to that of the neat epoxy. The Ti64 powder content significantly influenced the thermal conductivity increase. Specifically, both powder samples A and B provided an improvement in the thermal conductivity of the resulting composites. The composites containing B fillers also exhibited a little better thermal conductivity compared to the containing A fillers. The particle size has a significant impact on thermal conductivity, thus the disparity is most likely attributable to the dissimilar particle sizes between the two types of fillers. The result indicates that the usage of bigger particles leads to improved thermal conductivity of the composites by creating wider conductive paths, decreasing the interfacial phonon scattering between matrix and fillers. Improving the interface by increasing the Ti64 powder filler content would result in increased thermal conductivity by reducing phonon scattering at the interface, but increasing the filler ratio in matrix was not as effective as the use of larger particles [106].

### 3.3.5 TG Analysis of the Ti64 Powder Reinforced Epoxy Composites

Thermogravimetric (TG) curves in Fig. 3.14 were obtained in a thermobalance, Netzsch model TGA-50, using $Al_2O_3$ crucibles under conditions of dynamic nitrogen atmosphere (50 ml/min), sample mass of approximately 5 mg, and a heating rate of 10$^{o}$ C/min in the temperature range of 30 to 900 $^{o}$C. TGA experiments were conducted to determine the degradation temperatures of the Ti64 reinforced epoxy composite materials. The results of thermal degradation (Tdeg) values for the epoxy composites are shown in Table 3.7. The temperature corresponding to the peak in the first derivative of weight percent with temperature, reported as degradation temperature (Td), indicates the temperature corresponding to the highest rate of weight loss.

Table 3.7: Initial degradation temperatures of neat epoxy and Ti64 reinforced epoxy composites

| Sample | Td ($^{o}$C) |
|---|---|
| **Neat** | 323.75 ± 0.02 |
| **A3** | 324.47 ± 0.03 |
| **A5** | 325.48 ± 0.07 |
| **A10** | 327.92 ± 0.06 |
| **B3** | 325.30 ± 0.02 |
| **B5** | 327.83 ± 0.09 |
| **B10** | 329.20 ± 0.08 |

The results show that the samples with higher amount of Ti64 powder have higher temperature of thermal degradation and lower degradation rate in regard to the neat epoxy resin. These results confirmed that the thermal stability of the composites increased as the Ti64 powder loading increased. However, the difference in the sizes of the powder does affect the pattern of the thermal degradation profiles of both types of composites. As shown in Fig. 3.14, the mass loss step for the neat epoxy ended at approximately 600 °C. The mass loss step of the Ti64 powder reinforced epoxy composites ends above 650 °C due to the Ti64 powder have a higher thermal stability. After the mass loss step, the ash content for Ti64 powder reinforced epoxy composites is seen to be higher compared to the epoxy resin.

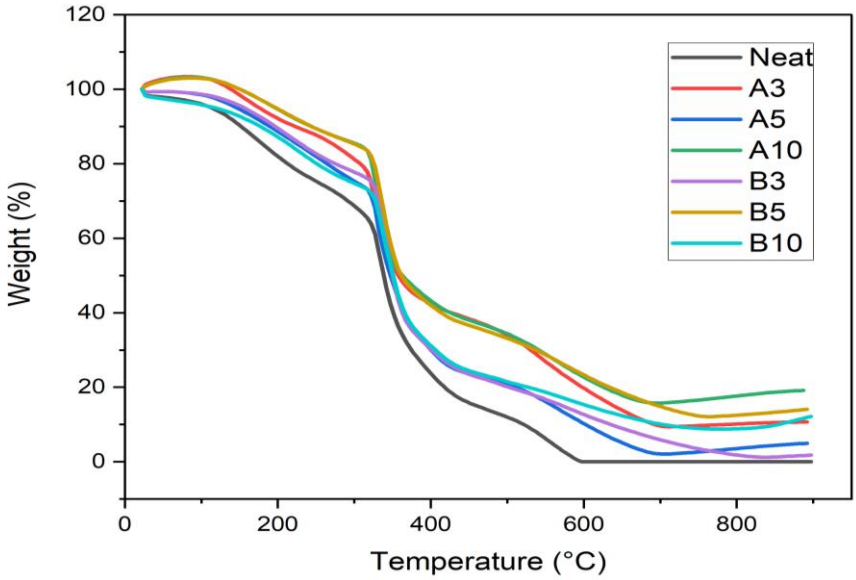


Figure 3.14: TGA graph of the neat epoxy and Ti64 reinforced epoxy composites

### 3.3.6 SEM Analysis of the Ti64 Powder Reinforced Epoxy Composites

Morphological analysis of the powders and specimens were characterized using a Carl Zeiss 300VP scanning electron microscope (SEM). SEM micrographs of the tensile fracture surfaces of neat epoxy resin and Ti64 powder reinforced epoxy composites are shown in Fig. 3.15 at 1kX magnification. The fractured surface of the neat resin was marked by stress lines. This shows that plastic deformation had occurred in the resin. The fractured surface reveals a smooth matrix surface, typical of a brittle fracture surface of the composite. The SEM test was conducted to examine the fractured region of tensile test specimens with Ti64 powder contents of 3-5-10%. In order to determine the homogeneity of Ti64 powder dispersion within polymeric matrices, fracture surfaces were prepared and examined via SEM. Ti64 powders, which are used as a reinforcing agent, were not homogeneously dispersed in the structure, and aggregation occurred. The tensile fracture surfaces of the Ti64 powder reinforced epoxy composites indicated that the majority of the Ti64 particles were embedded in the epoxy matrix, and that the Ti64 particles were dispersed in an inhomogeneous manner throughout the matrix. Particle traces formed during the tensile test can be seen as voids on the fracture surface. This indicates a strong interaction between the matrix and the particles.

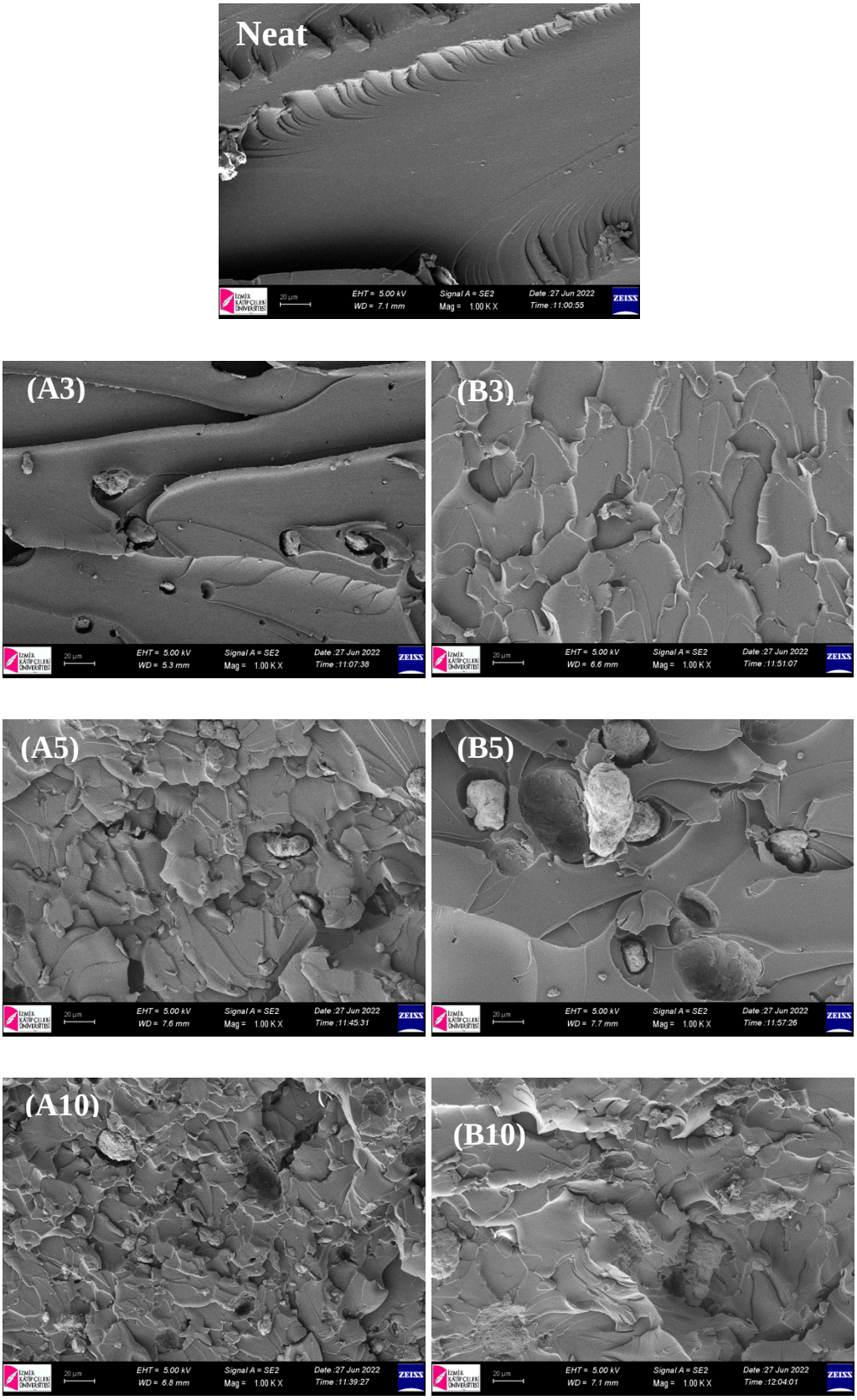


Figure 3.15: SEM micrographs of the tensile fracture surfaces of the epoxy composites

### 3.3.7 Effect of the Powder Oxygen Concentration in the Epoxy Composites

The oxygen concentrations of A and B Ti64 powders used as reinforcement in the epoxy composites are given in Table 3.3. Powder A with a low average particle size has a higher oxygen concentration than powder B. The oxidation level of the particles used as filler also affects the tensile and flexural properties of the composites [107]. The tensile and flexural strength of powder A filled epoxy composites increased when compared to powder B filled epoxy composites. However, one of the important parameter is the wettability between particle and resin interfaces. Chemical composition and surface chemistry (including surface oxidation) are some of the influencing factors, all strongly affecting the wettability. Strong interfacial bonding between reinforcements and resin may significantly improve the mechanical properties. High oxidation may be cause to achieving good particle-resin wettability [108-111].

Thermal conductivity results showed that oxygen concentration is one of the important factors. The thermal conductivity values of B3-B5-B10 composites with low oxygen content are higher than A3-A5-A10 composites. The presence of oxygen acts as vacancies in the composite. Vacancies are strong phonon scatterers. The thermal conductivity reduction can be attributed due to high oxygen content [112, 113].

## 3.4 Conclusions

The recycled Ti64 powder was used as reinforcement in epoxy composites for the first time. In this chapter, experimental studies were executed to evaluate the mechanical and microstructure properties of the epoxy composites filled within the range of 3-5-10wt % proportion of the recycled Ti64 powder.

- The tensile strength of the recycled Ti64 powder filled epoxy composites increased with increasing Ti64 proportion. The flexural strength of sample A is higher than that of sample B because the smaller particles have better dispersion, a larger surface area with the matrix.

- The filler content affected the thermal conductivity of the epoxy composite. The addition of Ti64 powder as reinforcement material to the polymer matrix significantly increases the thermal conductivity of the composite compared to that of the neat polymer.
- In addition to the physical properties of the powders such as particle shape and particle size, elemental composition of the powder also affects the mechanical and thermal properties of the composites.
- It is observed that the oxygen concentration of the powder has a decisive effect on the mechanical and thermal properties of the composites.
- TGA results show that Ti64 powder-reinforced composites have higher thermal degradation temperature and lower degradation rate compared to neat epoxy resin.

# Chapter 4

# Effects of Ti6Al4V Powder Properties on the Behaviors of Particle Reinforced Polyester Matrix Composites

## 4.1 Introduction

Composite materials, which first appeared in the middle of the 20th century, are currently one of the hottest areas of study in contemporary technology. They are ideal for several applications in the industrial sectors of aerospace, automotive, construction, sports, and bio-medicine, among many others, because to their promising properties.

Modern technologies frequently call for materials with very complex property combinations that are not possible with more traditional metal alloys, ceramics, and polymeric materials. This is particularly true of materials used in transportation, undersea, and aircraft applications. For instance, structural materials with low density, strength, stiffness, resistance to abrasion and impact, and resistance to corrosion are increasingly sought after by aircraft engineers. The combination of these qualities is quite strong. Strong materials are frequently relatively thick and increasing strength or stiffness typically causes a reduction in impact strength. [4]. These materials have exceptional mechanical and structural qualities, including a high strength-to-weight ratio, resistance to fire, chemicals, corrosion, and wear, as

well as being inexpensive to produce [114, 115]. Composites are classified based on the morphology of reinforcement (fiber, particulate reinforced and laminate composites) or the matrix material (metal, ceramic, polymer matrix composite). In a polymer composite material, a matrix is a resin and the reinforcement is in the form of dispersed particles which acts as the second phase. A wide range of microstructures can be obtained with combinations of matrix material and reinforcement. The relation between the properties and the structure of two-phase materials has been studied in the past decades by many authors. In commercial production, low-cost particulate fillers are added to plastics primary reason being economic and improvements in molding characteristics. It is not only the material properties of the two components or the volume fraction of the filler which governs the deformation behavior but the shape, size, orientation and the state of adhesion between the filler and the matrix also govern it [116].

Polyester resins and other thermosetting plastics are frequently utilized as matrix materials because they evenly distribute stresses in all directions and can withstand shocks and vibration. The most used resin system is polyester resin, notably in the marine industry. The liquid mixtures of low molar mass reactants, such as monomers, that are used to make thermosetting plastics polymerize to form strongly cross-linked network polymers [117-119]. The qualities of the particle filler dispersed in composite are enhanced. They have been able to find significant uses as high-strength, low-weight materials thanks to polymer composites created in this way. Polymer matrix composites can be reinforced with fibers (synthetic or natural), whiskers, and particulate materials. Natural fillers include minerals such as calcium carbonate, mica, talc, and some agricultural by products while synthetic fillers include processed mineral products such as carbon black, fumed silica, and aluminum hydroxide [120, 121]. The sizes of particulate fillers range from 0.1μm to about 2 mm. It is shown from the literature that the research on Ti64 powder-reinforced polymer composites is quite limited.

In recent years nonmetals are used as reinforcement in a polymer composite, and metal particles are prospective reinforcing material for various composites. Composites are possible to develop with minimal overall production cost by

embedding waste metal particles from other manufacturing processes or recycled materials in a polymer.

This study is concerned with the evaluation of mechanical properties such as tensile and flexural strength for different weight ratios of Ti64 particulate and polyester composite. Titanium alloys, which are especially preferred in aerospace applications, have tensile strength; creep and fatigue strength; fracture toughness; It contains α and β stabilizing elements to obtain the necessary mechanical properties such as fatigue cracking, stress-abrasion cracking, and oxidation resistance.

In this chapter, the flexural properties of Ti64 particle-reinforced polyester composites are studied through a three-point bend test, in which a loading nose deflects a specimen at a set span and loading rate until fracture. Three weight fractions of Ti64 particles 0%, 5%, and 10% were chosen to be studied.

## 4.2 Materials and Method

Ti64 alloy powder was utilized as reinforcement which was recycling powder obtained after mechanical milling. Ti64 powder of irregular shape was used in this study. The characteristics of recycled Ti64 powder used as reinforcement are given in detail in chapter 3. Two kinds of recycled Ti64 powder fillers with mean particle sizes of 15.4 μm and 34.6 μm were used. The average particle size distribution of the recycled Ti64 powder are given in Table 3.3. Commercial Ti64 powder of 15-45 μm was also used for comparison in the same parameters. Commercial Ti64 powder was obtained from Nanokar Company (Istanbul, Turkey). Table 4.1 shows the oxygen concentration in the recycled A and B powders and the commercial Ti64 powder. The oxygen ratios in the powders used in the study were measured using the LECO TC400 instrument.

Table 4.1: The oxygen concentration in the recycled A and B powders and the commercial Ti64 powder

| **Powder** | **Oxygen (ppm)** |
|---|---|
| A | 34840 |
| B | 20966 |
| Commercial | 2565 |

SEM images of the commercial and recycled Ti64 powders are given in Fig. 4.1. The morphology of the recycled powders is rounded and there are satellite nanoparticles on the particles. The commercial Ti64 particles shape is angular and has a smoother morphology than recycled Ti64 particles. We mentioned in the previous section that the morphology of the particles has an effect on the mechanical and thermal properties.

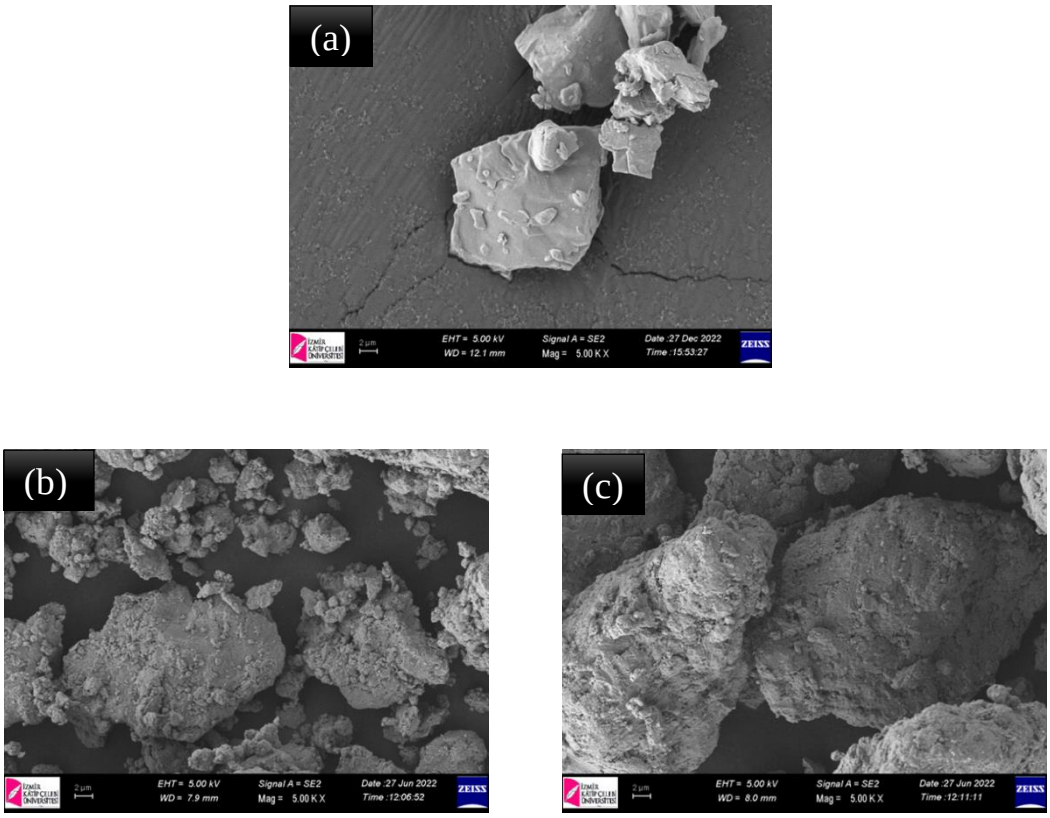


Figure 4.1: Particle morphology of the commercial powder (a), powder A (b), powder B (c)

A commercially available KP casting type polyester resin was used as the matrix material. It is a thermoset type of polymer matrix material. KP casting type polyester resin is an orthophthalic unsaturated polyester resin developed for general-purpose standard casting applications. The polyester resin was KP50 with added cobalt accelerator, which was used together with the hardener; both were purchased from Yücel Kompozit (Izmir, Turkey), given in Table 4.2. Methyl Ethyl Ketone Peroxide KP50 is used for curing general-purpose unsaturated polyesters at room temperature. It is generally added into the resin at a rate of 1-2% (by weight).

Table 4.2: Utilized the unsaturated polyester specifications

| | |
|---|---|
| **Appearance** | Transparent |
| **Colour** | Clear |
| **Density** | 1,11 g/cm³ |
| **Flash point** | 32 °C |
| **MEK-P hardener KP50** | % 1-2 |
| **Usable life** | 30 min / 25°C |
| **Cure time** | 12 hour / 25°C |

The polyester and hardener (%1-2) were mixed according to the datasheet provided by the supplier. Four formulations ranging from 0, 5 to 10 wt% Ti64 powder in polyester were developed as summarized in Table 4.3. The mean particle sizes of the powders which are dispersed by a range of dry units were determined using a laser diffraction particle size measurement instrument (Malvern Mastersizer 3000).

Table 4.3: The composition ratio of Ti6Al4V powder in the polyester composite

| Sample code | Mean particle size (µm) | Polyester (wt%) | Ti64 powder (wt%) | Powder type |
|---|---|---|---|---|
| **Neat** | unfilled | 100 | 0 | - |
| **PA5** | 15.4 | 95 | 5 | Recycled |
| **PA10** | 15.4 | 90 | 10 | Recycled |
| **PB5** | 34.6 | 95 | 5 | Recycled |
| **PB10** | 34.6 | 90 | 10 | Recycled |
| **PC5** | 15-45 | 95 | 5 | Commercial |
| **PC10** | 15-45 | 90 | 10 | Commercial |

A specially designed and fabricated silicon mould is used for this purpose to avoid stick during curing, as given in Fig. 3.1.

Ti64 powder was oven-dried for 24 h at 80 $^{0}$C. Ti64 powder was mixed with polyester using a low speed stirred mechanically to avoid bubbles and hardener was mixed into the mixture of Ti64 powder/polyester resin. In synthesizing the reinforced polyester composites, the mass of the polyester was varied with that of the reinforcement to give a total of 40 g (as given in Fig. 4.2).

In case of particulate reinforced composites, Ti64 powder is added to the polyester resin first and mixed well in continuous stirring process until a uniform mixture was observed then the hardener is added with the Ti64/polyester mixture. Stirring of the mixture continues for a certain duration based on the exothermic reaction. The neat polyester resin samples were also prepared under similar processing conditions, but without Ti64 powder.

Figure 4.2: Synthesizing the Ti64 powder reinforced polyester composites

The three-point bending test was performed with a constant loading speed of 1 mm/min at room temperature, and a span length of 102,4 mm as per ASTM D790 using a Shimadzu universal testing machine. The dimensions of the specimens are 125 mm ×12.7 mm × 3.2 mm with a span of 102.4 mm length (Fig. 3.3). A fixed span-to-depth ratio of 32 was used.

Laboratory tests were performed using the universal tensile strength testing machine Shimadzu (AG-IC 100kN) loading speed of the deformation corresponded to 1 mm/min at room temperature. Tensile test specimen dimension according to American Society for Testing and Materials (ASTM) D638-03 Type I is given in Fig. 3.4.

## 4.3 Results and Discussion

Five specimens of each type were tested. The results were averaged from five tests. All of the samples of types neat and PA-PB-PC for all cases of filler weight fractions and sample dimensions were successfully produced with no visible defects or other problems. Standard deviation values of tensile and bending test results are high as each sample is produced by hand.

### 4.3.1 Tensile Test Results

After the tensile strength analysis, the fracture regions are given in the Fig. 4.3. Moreover, Fig. 4.5 and Table 4.4 show the effect of adding different wt% and particle size of Ti64 powder on the tensile strength of polyester composites.

Figure 4.3: Tensile strength testing of the polyester composites with the fracture regions

The mechanical properties of particulate–polymer composites depend on the particle loading, particle size, and particle–matrix interface adhesion [122]. From Fig. 4.5 can be noticed that the tensile strength of the Ti64 powder-reinforced polyester composites, except for the PC5 composite, increases when compared to the neat polyester composite. It is clear that tensile strength is powerfully dependent on particle proportion. Based on the results from the Shimadzu (AG-IC 100kN) machine, the values of Young's modulus of the composites were given in Table 4.4.

Table 4.4: Tensile strength of polyester reinforced with different wt% of Ti6Al4V powder

| Sample | Tensile Strength (N/mm$^2$) | Young's Modulus (GPa) |
|---|---|---|
| Neat | 44.83 ±2.46 | 1.21 |
| PA5 | 47.42 ±4.20 | 1.17 |
| PA10 | 62.17 ±3.16 | 1.92 |
| PB5 | 49.35 ±4.02 | 1.35 |
| PB10 | 55.38 ±3.34 | 1.39 |
| PC5 | 43.58 ±2.22 | 0.99 |
| PC10 | 52.67 ±2.71 | 1.48 |

In Fig. 4.4, the polyester composites show decreasing strain (ductility) as Ti64 concentration increases. The lowest strain values were obtained PA10 sample. The proportion of the particles filled in PMC is important to the general mechanical behavior of the composite. On the other hand, extreme particle adding is easy to cause agglomeration of the fillers and therefore introduces defects to the matrix [123]. The tensile strength increases slightly when 5% by weight of the particles is added, while the tensile strength increases significantly when 10% by weight of the particles is added polyester resin. If there is an improvement in tensile strength as the particle proportion increases, there is strong interfacial bonding between the particle and the matrix. The particle size is also a parameter that affects the mechanical properties of the filled matrix [124].

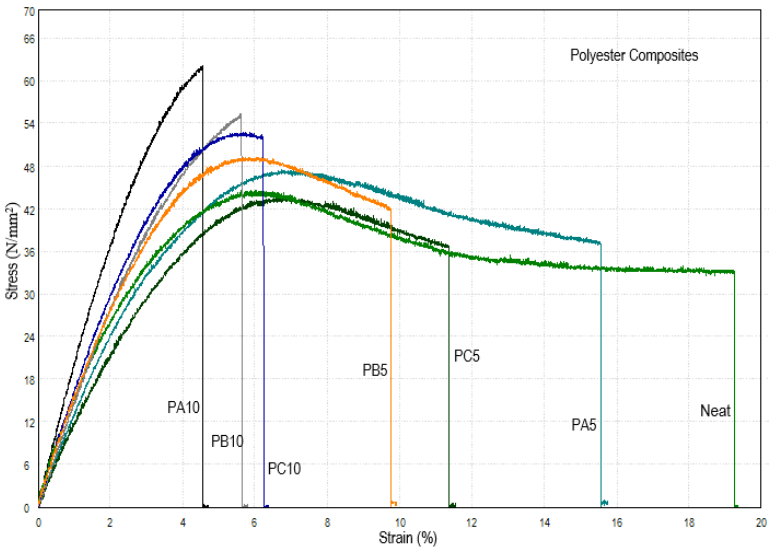


Figure 4.4: Tensile stress-strain curves of the polyester composites

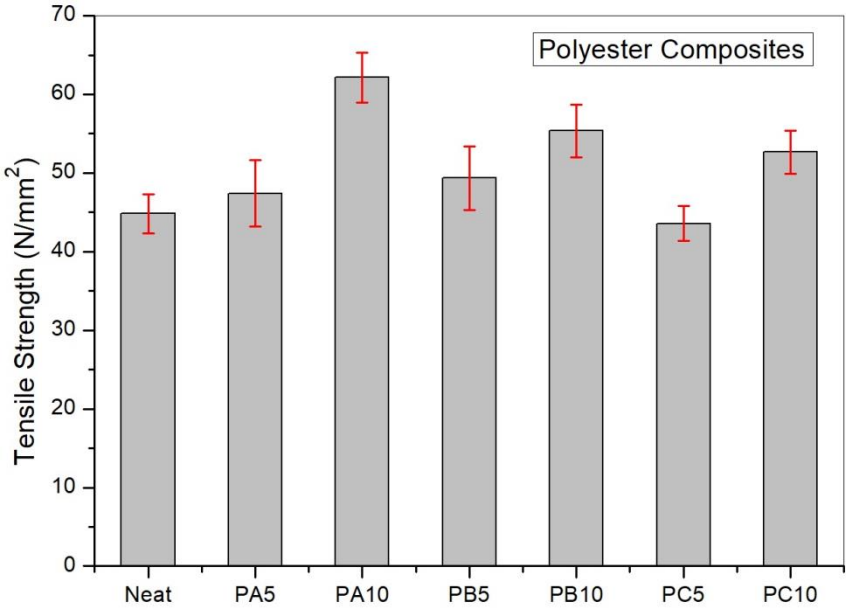


Figure 4.5: Tensile strength test graph of the polyester composites

The tensile strength also increased given the same weight fraction of the fillers as the particle size decreased due to the increased interfacial area between the particle surface and polymer matrix. The commercial Ti64 powder as reinforcement was used in PC5 and PC10 composites produced with the same parameters. The tensile strength of the commercial Ti64 powder-reinforced composites is lower than the recycled Ti64 powder-reinforced polyester composites. It is known that the particle shape affects the mechanical behavior in PMC [124]. The commercial Ti64 powder has a more regular morphology than the recycled Ti64 powder. The irregularly shaped reinforcement connects with the matrix in an interlocking manner [125].

### 4.3.2 Three Point Bending Test Results

The flexural strength of particle-reinforced polymer matrix composite is affected by factors such as the bonding strength between the particles and the matrix, particle size, and particle loading. The bending test is a simple supports test method that involves a three-point bending test, in which is loading pin is lowered from above at a constant rate. The specimen is placed on two supporting pins a set distance a part specimen, that fixture on a universal testing machine at a cross head speed and applied load which was gradually loaded until the breakage of the specimen occur (Fig. 4.6).

Figure 4.6: The universal three point bending testing machine

Details of the test preparation, conditioning, and load rate affect the test results. An average of five specimens was taken. Table 4.5 and Fig. 4.7 show the effect of adding Ti64 powder with different weight fractions on the flexural strength and flexural modulus of polyester composites.

Table 4.5: Flexural strength of the polyester composites

| Sample | Flexural Strength ($N/mm^2$) | Flexural Modulus (MPa) |
|---|---|---|
| Neat | 106.61 ±2.44 | 2.280 |
| PA5 | 103.92 ±4.58 | 2.525 |
| PA10 | 118.33 ±3.71 | 2.945 |
| PB5 | 101.78 ±4.40 | 1.973 |
| PB10 | 135.85 ±3.03 | 3.098 |
| PC5 | 93.54 ±3.82 | 1.956 |
| PC10 | 104.09 ±2.87 | 2.774 |

The results indicated that the flexural strength decreased at the particle incorporating 5 wt% and then followed an increasing with further particle content of 10 wt%. For the composites PA5-PB5-PC5 with a reinforcement ratio of 5 wt%, the decreased flexural strength led to a reduction in bending stress. This may be a result of poor bonding of the particles with the matrix and the inhomogeneous filling of reinforcement in matrices (poor particle distribution) that diminished the support to bending stress. The particles debond easily when the composite is subjected to load,

which could lead to the formation of large voids [126]. The flexural strength values of the PA10-PB10-PC10 composites were significantly enhanced compared with the unfilled polyester composite due to good particle dispersion and strong polymer/filler interface adhesion for effective stress transfer [127, 128]. These results imply that the particle proportion has great effect on composite strength. For the particulate composites, the flexural strength depends on the transferring stress between the matrix and particles [129]. The highest improvement of flexural strength was obtained at 10 wt% content of PB10. The lowest flexural strength of the composites with 10% particle proportion was obtained in the PC10 composite.

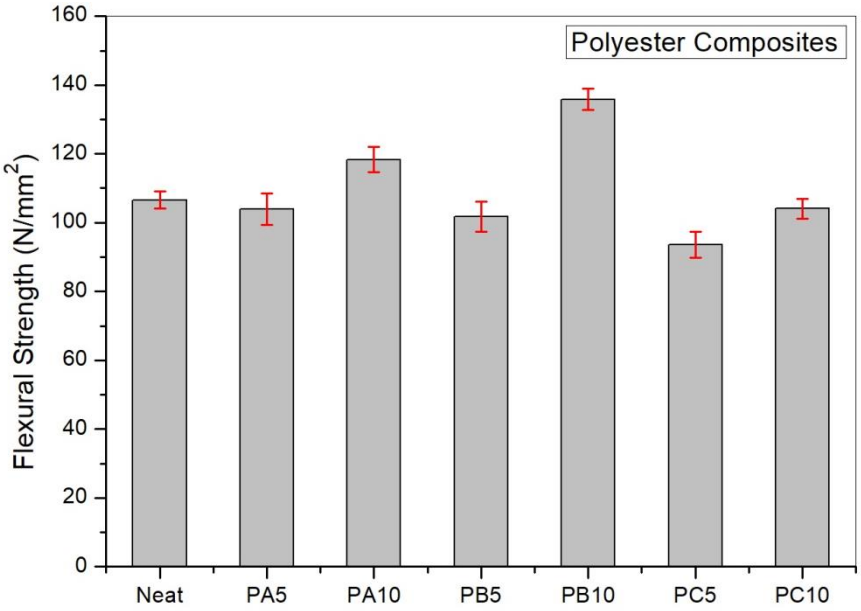


Figure 4.7: Flexural strength results of the polyester composites

### 4.3.3 Thermal Conductivity Test Results

The experimental results of the thermal conductivity are presented in Table 4.6. The effective thermal conductivity of a composite material composed of one type of filler introduced into a polymer matrix depends on the thermal conductivity of the components, the filler's shape, size, and concentration, their dispersion into the polymer, and the thermal interfacial resistance [85].

The addition of the recycled Ti64 powder to the polyester matrix slightly reduced the thermal conductivity of the composite over that of the neat polymer. However, the incorporation of the commercial Ti64 powder filler in the polyester matrix considerably increased the thermal conductivity of PC5-PC10 composites. In the

previous sections, the properties of Ti64 powders used as fillers were mentioned. The morphology of the commercial Ti64 powder is regular than the recycled Ti64 powder. Thus, the Ti64 filler particle shape and the distribution of filler particles are the critical factors controlling the thermal properties of metal-filled composites. The result is most likely due to the different particle shape between the commercial and recycled types of filler since the particle shape have a substantial effect on thermal conductivity [130].

Table 4.6: The experimental results of the thermal conductivity measurements

| Sample | Thermal conductivity (W/mK) |
|---|---|
| Neat | 0.2502 ±0.001 |
| PA5 | 0.2271 ±0.003 |
| PA10 | 0.2317 ±0.003 |
| PB5 | 0.2121 ±0.001 |
| PB10 | 0.2344 ±0.003 |
| PC5 | 0.6079 ±0.020 |
| PC10 | 0.6319 ±0.010 |

### 4.3.4 Morphology of the Composites

The fracture surfaces of neat polyester and the Ti64 particle reinforced composite samples were investigated various fracture features under scanning electron microscope. According to Fig. 4.8, the results of the experiment also show the irregular stratification of filler microparticles in the matrix. According to this observation, the quality of powder-matrix mixing process was not sufficient and better mixing might improve the powder dispersion in matrix. Brittle type fracture mode was observed in all polyester composite samples. However, micron-sized voids formed by the particles were observed on the fracture surfaces. When applying the particles to the matrix, the wetting of the particles with the matrix is very important. The presence of particle traces on the fracture surfaces indicates that the particles are held by the matrix material.

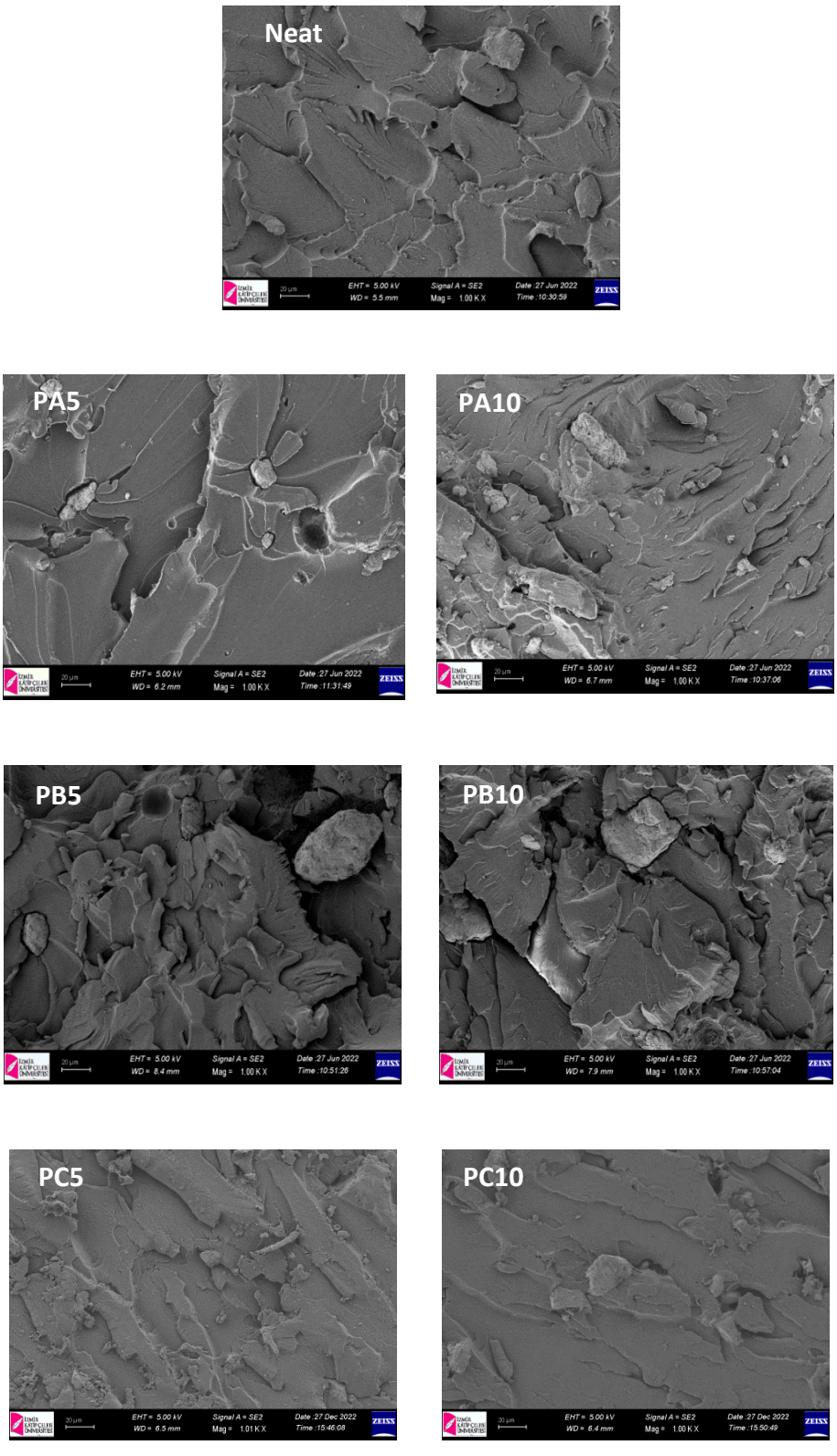


Figure 4.8: Morphology of the polyester composite specimens at different magnifications

### 4.3.5 Effect of the Powder Oxygen Concentration

We focused oxygen effects on the mechanical properties in the polyester composites. The measured oxygen concentrations in the A, B and commercial Ti64 powder were 34840 ppm, 20966 ppm, and 2565 ppm, respectively. The results show that the powder oxygen concentration has a significant effect on the mechanical properties of the Ti64 powder-reinforced polyester composites. The tensile and flexural strength of PC samples decrease compared to PA-PB samples with high oxygen concentrations. High oxidation may be cause to achieving the strong particle-matrix adhesive bonding. In general, high oxide concentrations can provide strong particle-matrix interfacial bonding [131, 132].

The oxidation level of the particles used as filler also affects the thermal properties of the composites. Although high oxygen content improves mechanical properties, it has a negative effect on thermal conductivity. Thermal conductivity decreases in PA and PB composites due to the high oxygen content. However, a significant increase in thermal conductivity is observed in PC samples with low oxygen content. Specifically, the thermal conductivity increases with decreasing the oxidation level. The presence of high oxygen causes with a reduced thermal conductivity because of the reduced of phonon scattering. Phonon scattering from grain boundaries and internal defects is an important factor affecting thermal conductivity. The presence of high oxygen causes with a reduced thermal conductivity because of the reduced of phonon scattering. As a result, the thermal conductivity determined at high oxidation levels is lower than at low oxidation levels [133-135].

## 4.4 Conclusion

In this section, the effect of particle size, shape and filler content on the mechanical behavior of polymer matrix composites reinforced with the recycled and commercial Ti64 powder is investigated. The composites loaded at different filler weight fractions were manufactured, mechanically characterized. The main conclusions can be summarized as follows:

- With the filler loading, an increase in the tensile strength was achieved.

- A small decrease in bending strength with filler weight fraction 5% was observed. However, an increase in flexural strength was observed with 10% filler weight fraction.
- The addition of the recycled Ti64 powder to the polyester matrix slightly reduced the thermal conductivity of the composite over that of the neat polymer. However, the incorporation of the commercial Ti64 powder fillers in the polyester matrix considerably increased the thermal conductivity of the composites.
- The effects of the oxygen content of the powders used as reinforcement on the mechanical and thermal properties of the composite were investigated. Since the powder oxygen content forms a strong particle matrix bond, it has an improving effect on the mechanical properties. However, it is observed that the increase in the oxygen ratio decreases the thermal conductivity of the composites.

# Chapter 5

# General Conclusion

This thesis aims to manufacture the Ti64 alloy chip that emerged after the machining process into powder form by using the mechanical milling method and the use of the recycled Ti64 powder as reinforcement in polymer composites was investigated.

- In the first chapter of the thesis, the properties of polymer composites and the characteristics of the particles used as fillers are summarized.
- In the second chapter, the particle size distribution, phase analysis, morphology, and elemental contents of the recycled Ti64 powders produced in various milling parameters such as the milling atmosphere, milling speed, and milling duration were characterized. As the milling speed and duration increased, the particle size decreased. Milling speed and duration affect the particle morphology. It is observed that as the milling speed and duration increase, the particle shape becomes more rounded. The particle morphologies of DAR powders are more rounded than DAT powders as a result of the milling process in argon atmosphere. In addition, agglomeration and small particles attached to the surface of larger particles are observed in DAT powders. As the milling duration and speed increased, the crystallite size of the powders decreased in proportion to the mean particle size. The bulk density of DAT-coded powders is lower than that of the DAR-coded powders because of the DAT-coded powders' more irregular particle morphology and lower average particle size characteristics.
- In the third chapter, the recycled Ti64 powder was used as reinforcement material in the epoxy composites. The mechanical properties and microstructure of the Ti64 powder-reinforced epoxy composites produced with different particle sizes and ratios by weight fraction were investigated.

Powder shape and size, powder content in matrix affect the mechanical and thermal properties of the epoxy composite. The oxygen concentration in the powders also affects the mechanical and thermal properties. The tensile strength of the recycled Ti64 powder filled epoxy composites increased with increasing the Ti64 powder proportion. The flexural strength of A samples is higher than that of B samples because the smaller particles have better dispersion, a larger surface area with the matrix. The addition of the Ti64 powder as reinforcement material to the polymer matrix significantly increases the thermal conductivity of the composite compared to that of the neat polymer. High oxygen content of the powder improves the mechanical properties of the epoxy composites but decreases the thermal conductivity.

- In the fourth part of the thesis, the recycled and commercial Ti64 powder was added to polyester composites at different filling ratios by weight fraction. By examining the mechanical and microstructural properties of polyester composites, the effects of the Ti64 powder proportion by weight fraction and particle size parameters were investigated. With the filler loading, an increase in the tensile strength of the composites was achieved. A small decrease in flexural strength with filler weight fraction 5% was observed. The addition of the recycled Ti64 powder to the polyester matrix slightly reduced the thermal conductivity of the composite over that of the neat polymer. However, the incorporation of the commercial Ti64 powder fillers in the polyester matrix considerably increased the thermal conductivity of the composites. The presence of high oxygen in the powder causes with a reduced thermal conductivity of the composites because of the reduced of phonon scattering.

The recycling of Ti64 chip is likely to provide both ecological and economic benefits. In this thesis, the Ti64 chip, which are converted into powder form, are included in the production processes in the context of circular economy. It was concluded that the recycled Ti64 powder are suitable for use as fillers in polymer composites. In addition, the characteristic results of the recycled powder show that it can be used in powder metallurgy.

# References


1. Campbell, F.C., *Structural composite materials*. 2010: ASM international.

2. Strong, A.B., *Plastics: materials and processing*. 2006: Prentice Hall.

3. Peng, W. and B. Riedl, *Thermosetting resins.* Journal of chemical education, 1995. **72**(7): p. 587.

4. Callister, W.D. and D.G. Rethwisch, *Materials science and engineering: an introduction*. Vol. 9. 2018: Wiley New York.

5. Mohammed, M.A., *Mechanical behavior for polymer matrix composite reinforced by copper powder*. Al-Nahrain Journal for Engineering Sciences, 2011. **14**(2): p. 160-176.

6. Gupta, N. and M. Paramsothy, *Metal-and polymer-matrix composites: functional lightweight materials for high-performance structures.* JOM, 2014. **66**(6): p. 862-865.

7. Fu, S.-Y., et al., *Effects of particle size, particle/matrix interface adhesion and particle loading on mechanical properties of particulate–polymer composites.* Composites Part B: Engineering, 2008. **39**(6): p. 933-961.

8. Pleşa, I., et al., *Properties of polymer composites used in high-voltage applications.* Polymers, 2016. **8**(5): p. 173.

9. Nichols, G., et al., *A review of the terms agglomerate and aggregate with a recommendation for nomenclature used in powder and particle characterization.* Journal of pharmaceutical sciences, 2002. **91**(10): p. 2103-2109.

10. Basim, G.B. and M. Khalili, *Particle size analysis on wide size distribution powders; effect of sampling and characterization technique.* Advanced Powder Technology, 2015. **26**(1): p. 200-207.

11. Dubois, I., et al. *Correlation between particle size and surface area for chlorite and K-feldspar*. in *Water-Rock Interaction. B. Torres-Alvarado. London, Taylor & Francis Group*. 2010.

12. Daraio, D., G. Raso, and M. Marigo, *Particle Technology and Engineering: An Engineer's Guide to Particles and Powders: Fundamentals and Computational Approaches.* Johnson Matthey's international journal of research exploring science and technology in industrial applications, 2017: p. 227.

13. Allen, T., *Particle size measurement*. 2013: Springer.

14. Landel, R.F. and L.E. Nielsen, *Mechanical properties of polymers and composites*. 1993: CRC press.

15. Peters, S.T., *Handbook of composites*. 2013: Springer Science & Business Media.

16. Moses, Y., I. Simon, and I. Maxwell, *Mechanical properties of carbon fibre and metal particles filled epoxy composite.* International Journal of Emerging Technology and Advanced Engineering, 2008. **3**(11): p. 664-667.

17. Tekce, H.S., D. Kumlutas, and I.H. Tavman, *Effect of particle shape on thermal conductivity of copper reinforced polymer composites.* Journal of reinforced plastics and composites, 2007. **26**(1): p. 113-121.

18. Amoabeng, D. and S.S. Velankar, *Bulk soldering: Conductive polymer composites filled with copper particles and solder.* Colloids and Surfaces A: Physicochemical and Engineering Aspects, 2018. **553**: p. 624-632.

19. Bigg, D.M., *Mechanical, thermal, and electrical properties of metal fiber-filled polymer composites.* Polymer Engineering & Science, 1979. **19**(16): p. 1188-1192.

20. Veiga, C., J. Davim, and A. Loureiro, *Properties and applications of titanium alloys: a brief review.* Rev. Adv. Mater. Sci, 2012. **32**(2): p. 133-148.

21. Committee, A.I.H., *Properties and selection: nonferrous alloys and special-purpose materials.* ASM international, 1992. **2**: p. 1143-1144.

22. Froes, F., *Titanium: physical metallurgy, processing, and applications*. 2015: ASM international.

23. Donachie, M.J., *Titanium: a technical guide*. 2000: ASM international.

24. Wessel, J.K., *The handbook of advanced materials: enabling new designs*. 2004: Wiley Online Library.

25. Jackson, M.J. and W. Ahmed, *Surface engineered surgical tools and medical devices*. 2007: Springer.

26. Takeda, O., T. Ouchi, and T.H. Okabe, *Recent progress in titanium extraction and recycling.* Metallurgical and Materials Transactions B, 2020. **51**(4): p. 1315-1328.

27. Takeda, O. and T.H. Okabe, *Current status of titanium recycling and related technologies.* Jom, 2019. **71**(6): p. 1981-1990.

28. James, W., *Powder Metallurgy Methods and Applications, vol. 7.* ASM International, 2015.

29. Suryanarayana, C., *Mechanical alloying and milling.* Progress in materials science, 2001. **46**(1-2): p. 1-184.

30. Suryanarayana, C., *Mechanical Alloying and Milling Marcel Dekker*. Ee. Uu, 2004: p. 59-78.

31. Neikov, O.D. and N. Yefimov, *Handbook of non-ferrous metal powders: technologies and applications*. 2009: Elsevier.

32. Chakraborty, S., W. Moeder, and K. Yoshioka, *Plant Immunity.* 2017.

33. Sharma, M., et al., *Titanium foam through powder metallurgy route using acicular urea particles as space holder.* Materials letters, 2011. **65**(21-22): p. 3199-3201.

34. Mikli, V., et al., *Characterization of powder particle morphology.* Proceedings of the Estonian Academy of Sciences: Engineering(Estonia), 2001. **7**(1): p. 22-34.

35. Gurrappa, I., *Characterization of titanium alloy Ti-6Al-4V for chemical, marine and industrial applications.* Materials characterization, 2003. **51**(2-3): p. 131-139.

36. Liang, Z., et al., *The effect of heat treatment on microstructure evolution and tensile properties of selective laser melted Ti6Al4V alloy.* Journal of Alloys and Compounds, 2019. **782**: p. 1041-1048.

37. Ming, W., et al., *Dynamic mechanical properties and machinability characteristics of selective laser melted and forged Ti6Al4V.* Journal of Materials Processing Technology, 2019. **271**: p. 284-292.

38. Peters, M., et al., *Titanium alloys for aerospace applications.* Advanced engineering materials, 2003. **5**(6): p. 419-427.

39. Facchini, L., et al., *Microstructure and mechanical properties of Ti-6Al-4V produced by electron beam melting of pre-alloyed powders.* Rapid Prototyping Journal, 2009.

40. Rack, H. and J. Qazi, *Titanium alloys for biomedical applications.* Materials Science and Engineering: C, 2006. **26**(8): p. 1269-1277.

41. Ojolo, S., et al., *Experimental determination of the effect of some straight biological oils on cutting force during cylindrical turning.* Matéria (Rio de Janeiro), 2008. **13**: p. 650-663.

42. Simsek, I. and D. Ozyurek, *An investigation of the effect of high-energy milling time of Ti6Al4V biomaterial on the wear performance in the*

*simulated body fluid environment.* Powder Metallurgy, 2017. **60**(5): p. 384-392.

43. Wang, B., et al., *Effect of milling time on microstructure and properties of Nano-titanium polymer by high-energy ball milling.* Applied Surface Science, 2018. **434**: p. 1248-1256.

44. Dikici, T. and M. Sutcu, *Effects of disc milling parameters on the physical properties and microstructural characteristics of Ti6Al4V powders.* Journal of Alloys and Compounds, 2017. **723**: p. 395-400.

45. Soufiani, A.M., M. Enayati, and F. Karimzadeh, *Fabrication and characterization of nanostructured Ti6Al4V powder from machining scraps.* Advanced Powder Technology, 2010. **21**(3): p. 336-340.

46. Goso, X. and A. Kale, *Production of titanium metal powder by the HDH process.* Journal of the Southern African Institute of Mining and Metallurgy, 2011. **111**(3): p. 203-210.

47. Wiatrowski, A., et al., *Comparison of the physicochemical properties of TiO2 thin films obtained by magnetron sputtering with continuous and pulsed gas flow.* Coatings, 2018. **8**(11): p. 412.

48. Xie, W., R. Li, and Q. Xu, *Enhanced photocatalytic activity of Se-doped TiO2 under visible light irradiation.* Scientific reports, 2018. **8**(1): p. 1-10.

49. Kang, S., et al., *Insights into the role of plasma in atmospheric pressure chemical vapor deposition of titanium dioxide thin films.* Scientific reports, 2018. **8**(1): p. 1-13.

50. Didwal, P.N., et al., *Intense field electron emission source designed from large area array of dense rutile TiO2 nanopillars.* Journal of Materials Science: Materials in Electronics, 2019. **30**(3): p. 2935-2941.

51. Xia, Y., et al., *Effect of calcined atmosphere on the photocatalytic activity of P-doped TiO2.* Applied Surface Science, 2014. **289**: p. 306-315.

52. Yan, M., et al., *Review of effect of oxygen on room temperature ductility of titanium and titanium alloys.* Powder metallurgy, 2014. **57**(4): p. 251-257.

53. Kozlík, J., et al., *Cryogenic milling of titanium powder.* Metals, 2018. **8**(1): p. 31.

54. Grell, W., et al., *Effect of powder oxidation on the impact toughness of electron beam melting Ti-6Al-4V.* Additive Manufacturing, 2017. **17**: p. 123-134.

55. Safdar, A., et al., *Evaluation of microstructural development in electron beam melted Ti-6Al-4V.* Materials Characterization, 2012. **65**: p. 8-15.

56. Abe, J., A. Popoola, and O. Popoola, *Consolidation of Ti6Al4V alloy and refractory nitride nanoparticles by spark plasma sintering method: Microstructure, mechanical, corrosion and oxidation characteristics.* Materials Science and Engineering: A, 2020. **774**: p. 138920.

57. Rafi, H., et al., *Microstructures and mechanical properties of Ti6Al4V parts fabricated by selective laser melting and electron beam melting.* Journal of materials engineering and performance, 2013. **22**(12): p. 3872-3883.

58. Andersson, S., et al., *Phase analysis studies on the titanium-oxygen system.* Acta chem. scand, 1957. **11**(10): p. 1641-1652.

59. Sato, H., et al., *Baddeleyite-type high-pressure phase of TiO2.* Science, 1991. **251**(4995): p. 786-788.

60. Popov Jr, V.V., et al., *The effect of powder recycling on the mechanical properties and microstructure of electron beam melted Ti-6Al-4 V specimens.* Additive Manufacturing, 2018. **22**: p. 834-843.

61. Lu, C., J. Zhang, and Z. Li, *Structural evolution of titanium powder during ball milling in different atmospheres.* Journal of alloys and compounds, 2004. **381**(1-2): p. 278-283.

62. Dabhade, V.V., T.R. Mohan, and P. Ramakrishnan, *Synthesis of nanosized titanium powder by high energy milling.* Applied surface science, 2001. **182**(3-4): p. 390-393.

63. Popovich, A. and V. Sufiiarov, *Metal powder additive manufacturing*, in *New trends in 3D printing*. 2016, IntechOpen.

64. Freeman, R., *The flowability of powders-an empirical approach.* From Powder to Bulk, 2000. **2000**(3): p. 545-556.

65. Hart, A., *Effect of particle size on detergent powders flowability and tabletability.* Journal of Chemical Engineering and Process Technology, 2015. **6**(1): p. 215-218.

66. Leyva, N. and M. Mullarney, *Modeling pharmaceutical powder-flow performance using particle-size distribution data.* 2009.

67. Jan, S., R. Ambrose, and D. Saxena, *Effect of grinding action on the flowability of rice flour.* Journal of Food Measurement and Characterization, 2017. **11**(2): p. 801-811.

68. Cain, J., *Flowability Testing-An Alternative Technique fore Determining ANSI/CEMA Standard 550 Flowability Ratings for Granular Materials.* Powder Handling and Processing, 2002. **14**(3): p. 218-221.

69. Shi, H., et al., *Effect of particle size and cohesion on powder yielding and flow.* KONA Powder and Particle Journal, 2018: p. 2018014.

70. Basu, P., *Biomass gasification, pyrolysis and torrefaction: practical design and theory*. 2018: Academic press.

71. Neikov, O.D., D.V. Lotsko, and V.G. Gopienko, *Powder characterization and testing.* Handbook of Non-Ferrous Metal Powders: Technologies and Applications. Oxford: Elsevier, 2009.

72. Zhu, H., J. Fuh, and L. Lu, *The influence of powder apparent density on the density in direct laser-sintered metallic parts.* International Journal of Machine Tools and Manufacture, 2007. **47**(2): p. 294-298.

73. Breuer, O., *US, Big returns from small fibers: A review of polymer/carbon nanotube composites.* Polymer composites, 2004. **25**(6): p. 630.

74. Matthews, F.L. and R.D. Rawlings, *Composite materials: engineering and science*. 1999: Woodhead Publishing.

75. Xanthos, M., *Functional fillers for plastics*. 2010: John Wiley & Sons.

76. Huda, N., et al., *The analysis of attitudes, subjective norms, and behavioral control on muzakki's intention to pay zakah.* International Journal of business and social science, 2012. **3**(22).

77. Bhagyashekar, M. and R. Rao, *Effects of material and test parameters on the wear behavior of particulate filled composites part 1: SiC-epoxy and Gr-epoxy composites.* Journal of reinforced plastics and composites, 2007. **26**(17): p. 1753-1768.

78. Gulrez, S.K., et al., *A review on electrically conductive polypropylene and polyethylene.* Polymer composites, 2014. **35**(5): p. 900-914.

79. Erden, S., et al., *Enhancement of the mechanical properties of glass/polyester composites via matrix modification glass/polyester composite siloxane matrix modification.* Fibers and polymers, 2010. **11**(5): p. 732-737.

80. Nelson, J.K. *Overview of nanodielectrics: Insulating materials of the future*. in *2007 Electrical insulation conference and electrical manufacturing expo*. 2007. IEEE.

81. Han, J. and R. Garrett. *Overview of polymer nanocomposites as dielectrics and electrical insulation materials for large high voltage rotating machines*. in *NSTI-Nanotech*. 2008.

82. Tanaka, T., G. Montanari, and R. Mulhaupt, *Polymer nanocomposites as dielectrics and electrical insulation-perspectives for processing technologies, material characterization and future applications.* IEEE transactions on Dielectrics and Electrical Insulation, 2004. **11**(5): p. 763-784.

83. Yamamoto, I., T. Higashihara, and T. Kobayashi, *Effect of silica-particle characteristics on impact/usual fatigue properties and evaluation of mechanical characteristics of silica-particle epoxy resins.* JSME International Journal Series A Solid Mechanics and Material Engineering, 2003. **46**(2): p. 145-153.

84. Nakamura, Y., et al., *Effect of particle size on fracture toughness of epoxy resin filled with angular-shaped silica.* Polymer, 1991. **32**(12): p. 2221-2229.

85. Nakamura, Y., et al., *Effects of particle size on mechanical and impact properties of epoxy resin filled with spherical silica.* Journal of applied polymer science, 1992. **45**(7): p. 1281-1289.

86. Tekce, H., D. Kumlutas, and I. Tavman. *Determination of the thermal properties of polyamide-6 (nylon-6)/copper composite by hot disk method*. in *Proceedings of the 10th Denizli material symposium*. 2004.

87. Kaushal, S., *Analysis of deformation behaviour and fracture features in glass-epoxy composites toughened by rubber and carbon additions.* Journal of materials science letters, 1992. **11**(2): p. 86-88.

88. Hussain, M., et al., *Effects of wet ball-milling on particle dispersion and mechanical properties of particulate epoxy composites.* Materials Letters, 1996. **26**(3): p. 177-184.

89. Goyanes, S., et al., *Yield and internal stresses in aluminum filled epoxy resin. A compression test and positron annihilation analysis.* Polymer, 2003. **44**(11): p. 3193-3199.

90. Tilbrook, M., R. Moon, and M. Hoffman, *On the mechanical properties of alumina–epoxy composites with an interpenetrating network structure.* Materials Science and Engineering: A, 2005. **393**(1-2): p. 170-178.

91. Marghalani, H.Y., *Effect of filler particles on surface roughness of experimental composite series.* Journal of Applied Oral Science, 2010. **18**: p. 59-67.

92. Józwik, J., et al., *Diagnostics of CNC machine tools in manufacturing process with laser interferometer technology.* Manufacturing technology, 2014. **14**(1): p. 23-30.

93. Deshmukh, S., et al., *Effect of particle size and concentration on mechanical and electrical properties of the mica filled PVC.* Journal of Minerals and Materials Characterization and Engineering, 2010. **9**(09): p. 831.

94. Salih, S.I., *Acoustic and mechanical properties of polymer composites reinforced by pre-deformed palm fiber.* Eng. & Tech. Journal, 2013. **31**(3): p. 484-499.

95. Jesson, D.A. and J.F. Watts, *The interface and interphase in polymer matrix composites: effect on mechanical properties and methods for identification.* Polymer Reviews, 2012. **52**(3): p. 321-354.

96. Mashabela, M., M. Maringa, and T. Dzogbewu, *Nanoparticulate reinforced composites and their application to additively manufactured TI6AL4V for use in the aerospace sector.* Manufacturing Review, 2022. **9**: p. 29.

97. Kawaguchi, T. and R.A. Pearson, *The effect of particle–matrix adhesion on the mechanical behavior of glass filled epoxies: Part 1. A study on yield behavior and cohesive strength.* Polymer, 2003. **44**(15): p. 4229-4238.

98. Reynaud, E., et al., *Nanofillers in polymeric matrix: a study on silica reinforced PA6.* Polymer, 2001. **42**(21): p. 8759-8768.

99. Zhu, Z.K., et al., *Preparation and properties of organosoluble polyimide/silica hybrid materials by sol–gel process.* Journal of Applied Polymer Science, 1999. **73**(14): p. 2977-2984.

100. Bhagat, S. and P.K. Verma, *Effect of graphite filler on mechanical behavior of epoxy composites.* International Journal of Emerging Technology and Advanced Engineering, 2013. **3**(2): p. 427-430.

101. Durowaye, S., et al., *Mechanical properties of particulate coconut shell and palm fruit polyester composites.* International Journal of Materials Engineering, 2014. **4**(4): p. 141-147.

102. Huang, X., P. Jiang, and T. Tanaka, *A review of dielectric polymer composites with high thermal conductivity.* IEEE Electrical Insulation Magazine, 2011. **27**(4): p. 8-16.

103. Bartsch, K., et al., *Material modeling of Ti–6Al–4V alloy processed by laser powder bed fusion for application in macro-scale process simulation.* Materials Science and Engineering: A, 2021. **814**: p. 141237.

104. Bolzoni, L., E.M. Ruiz-Navas, and E. Gordo, *Flexural properties, thermal conductivity and electrical resistivity of prealloyed and master alloy addition powder metallurgy Ti–6Al–4V.* Materials & Design (1980-2015), 2013. **52**: p. 888-895.

105. Gong, X., et al. *Powder-bed electron-beam-melting additive manufacturing: powder characterization, process simulation and metrology*. in *Proceedings of the ASME District F Early Career Technical Conference*. 2013.

106. Lee, G.-W., et al., *Enhanced thermal conductivity of polymer composites filled with hybrid filler.* Composites Part A: Applied science and manufacturing, 2006. **37**(5): p. 727-734.

107. Chen, J. and L. Li, *Effect of oxidation degree on the thermal properties of graphene oxide.* Journal of Materials Research and Technology, 2020. **9**(6): p. 13740-13748.

108. Eustathopoulos, N. and R. Voytovych, *The role of reactivity in wetting by liquid metals: a review.* Journal of materials science, 2016. **51**(1): p. 425-437.

109. Saiz, E., A. Tomsia, and R. Cannon, *Ridging effects on wetting and spreading of liquids on solids.* Acta Materialia, 1998. **46**(7): p. 2349-2361.

110. Xiao, P. and B. Derby, *Wetting of titanium nitride and titanium carbide by liquid metals.* Acta materialia, 1996. **44**(1): p. 307-314.

111. Rado, C., S. Kalogeropoulou, and N. Eustathopoulos, *Wetting and adhesion in metal-silicon carbide systems: the effect of surface polarity of SiC.* Scripta materialia, 1999. **42**(2): p. 203-208.

112. Klemens, P.G., *Phonon scattering by oxygen vacancies in ceramics.* Physica B: Condensed Matter, 1999. **263**: p. 102-104.

113. Barjasteh, E., N. Kar, and S. Nutt, *Effect of filler on thermal aging of composites for next-generation power lines.* Composites Part A: Applied Science and Manufacturing, 2011. **42**(12): p. 1873-1882.

114. Yan, D.-X., et al., *Efficient electromagnetic interference shielding of lightweight graphene/polystyrene composite.* Journal of Materials Chemistry, 2012. **22**(36): p. 18772-18774.

115. Sahmaran, M., V.C. Li, and C. Andrade, *Corrosion resistance performance of steel-reinforced engineered cementitious composite beams.* ACI Materials Journal, 2008. **105**(3): p. 243.

116. Rajak, D.K., et al., *Recent progress of reinforcement materials: a comprehensive overview of composite materials.* Journal of Materials Research and Technology, 2019. **8**(6): p. 6354-6374.

117. Mazuki, A.A.M., et al., *Degradation of dynamic mechanical properties of pultruded kenaf fiber reinforced composites after immersion in various solutions.* Composites Part B: Engineering, 2011. **42**(1): p. 71-76.

118. Velmurugan, G., et al., *Mechanical testing of hybrid composite material (Sisal and Coir).* International Journal of Scientific and Research Publications, 2014. **4**(7): p. 1-6.

119. Selvam, R., S. Ravi, and R. Raja. *Fabrication of SiC particulate reinforced polyester matrix composite and investigation*. in *IOP Conference Series: Materials Science and Engineering*. 2017. IOP Publishing.

120. Njoku, R., A. Okon, and T. Ikpaki, *Effects of variation of particle size and weight fraction on the tensile strength and modulus of periwinkle shell*

*reinforced polyester composite.* Nigerian journal of technology, 2011. **30**(2): p. 87-93.

121. Teh, P.L., *Development Of Core Layer Materials Using Particulate Filled Epoxy Composites [TK7870. 15. T261 2008 f rb]*. 2008, Universiti Sains Malaysia.

122. Fu, S.-Y. and B. Lauke, *Characterization of tensile behaviour of hybrid short glass fibre/calcite particle/ABS composites.* Composites Part A: Applied Science and Manufacturing, 1998. **29**(5-6): p. 575-583.

123. Fu, S. and B. Lauke, *Analysis of mechanical properties of injection molded short glass fibre (SGF)/calcite/ABS composites.* Journal of Materials Sciences and Technology, 1997. **13**(5): p. 389.

124. Tjong, S. and S. Xu, *Ternary polymer composites: PA6, 6/maleated SEBS/glass beads.* Journal of applied polymer science, 2001. **81**(13): p. 3231-3237.

125. Lee, C.H., A. Khalina, and S.H. Lee, *Importance of interfacial adhesion condition on characterization of plant-fiber-reinforced polymer composites: A review.* Polymers, 2021. **13**(3): p. 438.

126. Peng, X., et al., *Properties of natural fiber composites made by pultrusion process.* Journal of Composite Materials, 2012. **46**(2): p. 237-246.

127. Jain, K., S. Shit, and S. Jain, *Evaluation of mechanical & thermal properties of polypropylene—palm kernel nut shell powder composites for green roof technology.* Journal of Information, Knowledge and Research in Mechanical Engineering, 2013. **2**(2): p. 456-459.

128. Singha, A., A.K. Rana, and R. Jarial, *Mechanical, dielectric and thermal properties of Grewia optiva fibers reinforced unsaturated polyester matrix based composites.* Materials & Design, 2013. **51**: p. 924-934.

129. Uyor, U., et al., *Enhanced thermal and mechanical properties of polymer reinforced with slightly functionalized graphene nanoplatelets.* Journal of Testing and Evaluation, 2019. **47**(4): p. 2681-2692.

130. Mamunya, Y.P., et al., *Electrical and thermal conductivity of polymers filled with metal powders.* European polymer journal, 2002. **38**(9): p. 1887-1897.

131. Meng, X., et al., *Friction self-riveting welding between polymer matrix composites and metals.* Composites Part A: Applied Science and Manufacturing, 2019. **127**: p. 105624.

132. Li, Y., et al., *Experimental and theoretical investigation of laser pretreatment on strengthening the heterojunction between carbon fiber-reinforced plastic and aluminum alloy.* ACS applied materials & interfaces, 2019. **11**(24): p. 22005-22014.

133. Rumble, J., *CRC handbook of chemistry and physics.* 2017.

134. Balandin, A.A., *Thermal properties of graphene and nanostructured carbon materials.* Nature materials, 2011. **10**(8): p. 569-581.

135. Sonvane, Y., et al., *Length, width and roughness dependent thermal conductivity of graphene nanoribbons.* Chemical Physics Letters, 2015. **634**: p. 16-19.